Open access • Journal Article • DOI:10.1038/S42254-020-0199-Z

Physicochemical hydrodynamics of droplets out of equilibrium — Source link

Detlef Lohse, Xuehua Zhang

Institutions: Max Planck Society, University of Alberta

Published on: 01 Aug 2020

Topics: Transport phenomena

Physicochemical Hydrodynamics of Droplets out of Equilibrium: A Perspective Review

Detlef Lohse* and Xuehua Zhang†

May 11, 2020

Abstract

Droplets abound in nature and technology. In general, they are *multicomponent*, and, when out of equilibrium, with gradients in concentration, implying flow and mass transport. Moreover, *phase transitions* can occur, with either evaporation, solidification, dissolution, or nucleation of a new phase. The droplets and their surrounding liquid can be binary, ternary, or contain even more components, and with several even in different phases. In the last two decades the rapid advances in experimental and numerical fluid dynamical techniques has enabled major progress in our understanding of the physicochemical hydrodynamics of such droplets, further narrowing the gap from fluid dynamics to chemical engineering and colloid & interfacial science and arriving at a quantitative understanding of multicomponent and multiphase droplet systems far from equilibrium, and aiming towards a one-to-one comparison between experiments and theory or numerics.

This review will discuss various examples of the physicochemical hydrodynamics of droplet systems far from equilibrium and our present understanding of them. These include immiscible droplets in a concentration gradient, coalescence of droplets of different liquids, droplets in concentration gradients emerging from chemical reactions (including droplets as microswimmers) and phase transitions such as evaporation, solidification, dissolution, or nucleation, and droplets in ternary liquids, including solvent exchange, nano-precipitation, and the so-called ouzo effect. We will also discuss the relevance of the physicochemical hydrodynamics of such droplet systems for many important applications, including in chemical analysis and diagnostics, microanalysis, pharmaceutics, synthetic chemistry and biology, chemical and environmental engineering, the oil and remediation industries, inkjet-printing, for micro- and nano-materials, and in nanotechnolgoy.

*d.lohse@utwente.nl, Physics of Fluids Group, Max-Planck Center for Complex Fluid Dynamics, MESA+ Research Institute and J.M. Burgers Centre for Fluid Dynamics, University of Twente, P.O. Box 217, 7500 AE Enschede, The Netherlands, and Max Planck Institute for Dynamics and Self-Organization, Am Fassberg 17, 37077 Göttingen, Germany

†xuehua.zhang@ualberta.ca, Department of Chemical and Materials Engineering, University of Alberta, Edmonton, AB T6G 1H9, Canada, and Physics of Fluids Group, Max-Planck Center for Complex Fluid Dynamics, MESA+ Research Institute and J.M. Burgers Centre for Fluid Dynamics, University of Twente, P.O. Box 217, 7500 AE Enschede, The Netherlands.

1 Introduction

Classical hydrodynamics focuses on pure liquids. In nature and technology, fluid dynamical systems are however *multicomponent*, and often with gradients in concentration, even changing in time, i.e., they are out of equilibrium. These concentration gradients, be they smooth or sharp, can induce a flow. Moreover, phase transitions can occur, with either evaporation, solidification, dissolution, or nucleation of a new phase. The liquids can be binary, ternary, or contain even more components, with several across different phases. The non-equilibrium can be driven by flow, mixing, phase transitions, chemical reactions, electrical current, heat, etc.

To theoretically deal with such systems, in the 1950s, Levich wrote the wonderful book "Physicochemical Hydrodynamics" [1]. The central theme of the book is the "elucidation of mechanisms of transport phenomena and the conversion of understanding so gained into plain, useful tools for applications," as L. E. Scriven describes it in the foreword to the book in its 1962 translation into English [1]. Levich can be viewed as a physical chemist and theoretical physicist at the same time, or, as Scriven puts it, above all, as an "engineering scientist" with a recognizable "blend of applied chemistry, applied physics, and fluid mechanics." V. Levich himself, in his foreword to the first Russian Edition (1952), describes the scope of physicochemical hydrodynamics as the "aggregate of problems dealing with the effect of fluid flow on chemicals or physicochemical transformations as well as the effect of physicochemical factors of the flow."

First and foremost, Levich's "Physicochemical hydrodynamics" is a book describing the relevant theoretical and mathematical concepts, given that in those days the experimental tools to actually measure the flow on the microscale were very limited and the possibility to perform direct numerical simulations of the underlying partial differential equations even absent. Today, more than 60 years later, the scientific and in particular the hydrodynamical and physicochemical communities have developed tremendously and the experimental, instrumental, and numerical means to actually deal with the problems Levich defined in his book have become available and are being used to do so.

These developments are more than timely, as the relevance of physicochemical hydrodynamics of multicomponent and multiphase liquids is ever increasing, in order to address the challenges of mankind for the 21st century. These challenges include energy, namely storage and batteries, hydrogen production by electrolysis, CO_2 capture, polymeric solar cell manufactering, biofuel production, and catalysis. They also include health and medical issues like chemical analysis and diagnostics or the production and purification of drugs, advanced material manufacturing, environmental issues like flotation, water cleaning, membrane management, and separation technology, or food processing and food safety issues. They also include issues in modern production technologies such as additive manufacturing on ever decreasing length scales and inkjet printing, and in the paint and coating industry.

These challenges have often been approached with a pure engineering approach, and less in the spirit of Levich as an engineering scientist. On the other hand, as said above, classical hydrodynamics has focused on pure and single-phase liquids. In the last two decades, the advent of new experimental and numerical tools has allowed for a more integrated understanding of physicochemical hydrodynamics and to further narrow the gap between classical hydrodynamics and chemical engineering and colloid & interfacial science. The objective of this effort is to improve the *quantitative* understanding of multicomponent and multiphase fluid dynamic systems far from equilibrium, in order to master and better control them. To achieve this objective, one has to perform controlled experiments and numerical simulations for idealized setups, allowing for a *one-to-one comparison* between experiments and numerics/theory, in order to test the theoretical understanding. This effort indeed is in the spirit of Levich's "Physicochemical Hydrodynamics", but now building on and benefiting from the developments of modern microfluidics, microfabrication, digital (high-speed) imaging technology, confocal microscopy, atomic force microscopy, and various computational techniques and opportunities for high-performance computing. These are, in a nutshell, the blessings from what can be considered as the golden age of fluid dynamics, which builds on the digital revolution, both on the experimental and the numerical side. Given these

developments, and given the necessity in chemical engineering to move towards higher precision and enhanced control, this effort is indeed very timely.

There is a large number of physical phenomena and effects which come into play in multicomponent and multiphase liquids far from equilibrium. These include gradients in concentration, either in the bulk of the liquid or on the surface, leading to diffusiophoresis and solutal Marangoni flow. They include (selective) dissolution of (multicomponent) droplets and bubbles in host liquids or vice versa their nucleation and growth. They also include the coalescence of droplets consisting of different liquids, possibly with chemical reactions and/or solidification and other transitions from one phase to another. The material parameters which become important are the various diffusivities and viscosities of the liquids, their surface tensions and how they depend on the concentrations, the volatilities and mutual solubilities, latent heats, reaction rates, etc.

Obviously, the field of multicomponent and multiphase hydrodynamics is too large to give an exhaustive review. So we restrict ourselves to small length scales, focusing on the physicochemical hydrodynamics of (multicomponent) droplets far from equilibrium. The objective of this perspective review is to show examples of such systems for which a successful quantitative description and one-to-one comparison between well-controlled table-top experiments and theory and numerics has been achieved, to identify the complex interplay of the underlying principles, and to put these examples into the context of relevant applications of multicomponent and multiphase liquid systems. In particular, we want to identify the new directions of physicochemical hydrodynamics and want to outline the scientific challenges and their connections with the technological challenges.

The core of the review is section 2. In the five subsections, we give general examples for the physicochemical hydrodynamics of (multicomponent) droplets far from equilibrium. In the five subsections of section 3 we give application fields and examples for the relevance of physicochemical hydrodynamics in technology. Finally, in section 4 we will try to identify the general lessons one learns from these examples and applications and will give an outlook to further directions and perspectives. For better readability, so that in the main sections we can better focus on the fluid dynamics and the physics, we have included three text boxes, namely one on the relevant dimensionless numbers in physicochemical hydrodynamics, one for the new experimental methods which have enabled the recent progress, and one on the new or improved numerical methods.

This perspective review convey ideas, rather than delve into detailed technical aspects or be encyclopedic. For these aspects we refer to specialized review articles on certain aspects, such as the one by Cates and Tjhung on binary fluid mixtures [2], by Lauga and Powers on swimmers [3], by Maass *et al.* on swimming droplets [4], by Moran and Posner and by Golestanian on phoretic self-propulsion [5, 6], by Manikantan and Squires on surfactant dynamics [7], by Cazabat & Guéna [8] and Erbil [9] on evaporation of pure liquid sessile droplets, by Sefiane on patterns from drying drops [10], by Lohse and Zhang on surface nanobubbles and nanodroplets [11], by Jain on single-drop microextraction [12], by de Wit on chemo-hydrodynamic patterns and instabilities [13], etc.

Box 1: Dimensionless numbers for droplets in physicochemical hydrodynamics
In fluid dynamics, it is common to express the ratio of the various forces (or time or length scales) in terms of dimensionless numbers. The most famous one is the

- **Reynolds number** $Re = UR/\nu$, which expresses the ratio of inertial forces to viscous forces. In the context of droplets, R is the droplet radius, U the (relative) droplet velocity, and ν the kinematic viscosity of the continuous phase.

In the context of the physicochemical hydrodynamics of droplets, which dissolve or grow, the perhaps even more relevant dimensionless parameter is the

- (diffusive) **Peclet number** $Pe = UR/D$, which compares the advective and diffusive time scales, where D is the mass diffusivity, which in general is much smaller than the viscosity ν, reflecting the very slow process of molecular diffusion in liquids.

The ratio between viscosity and diffusivity is the

- **Schmidt number** $Sc = \nu/D$, which correspondingly in physicochemical hydrodynamics is quite large, namely $\sim 10^3$, which on the one hand is the reason for many peculiarities in physicochemical hydrodynamics, and on the other hand introduces many experimental and numerical difficulties.

Once also thermal effects come into play, the thermal diffusivity κ will play a role. Its ratio to the molecular diffusivity and the kinematic viscosity is expressed as

- **Lewis number** $Le = \kappa/D$ and **Prandtl number** $Pr = \nu/\kappa$, which are typically ~ 400 and ~ 4, respectively, reflecting that the thermal diffusion is much faster than the molecular one, and that for standard liquids thermal transport is slightly slower than viscous transport.

In hydrochemical hydrodynamics, surface tension effects are crucial. They can be expressed either in terms of the

- **Weber number** $We = \rho U^2 R/\sigma$, which is the ratio of inertia to capillarity, where σ is the surface tension and ρ the density of the liquid, or the
- **Capillary number** $Ca = \eta U/\sigma$, ratio of viscous to capillary forces, or the
- **Ohnesorge number** $Oh = \eta/\sqrt{\rho_w \sigma R} = We^{1/2}/Re$, ratio of time of viscous damping to time of the capillary oscillations, or the
- **Bond number** $Bo = \rho g R^2/\sigma$, ratio of gravity to capillary forces.

The full richness of hydrochemical droplet fluid dynamics only enters once *several* liquids and gases come into play, with different surface tensions, densities, etc. Then the gradient of the hydrodynamic forces along or across a droplets introduces net forces. The most relevant may be the

- **Marangoni number** $Ma = R\Delta\sigma/(\rho\nu D)$, which compares the Marangoni forces with stabilizing viscous forces and stabilizing mass diffusion. The difference $\Delta\sigma$ in surface tension may be due to differences Δc in the composition of the liquid, where $c(\boldsymbol{x}, t)$ is the concentration field, or due to differences ΔT in the temperature of the liquid. Roughly, $\Delta\sigma \approx \partial\sigma/\partial c\, \Delta c$, and similarly for the temperature, but note that in general the dependence $\sigma(c)$ is very nonlinear [14]. In general, of course, $\sigma(T, c)$, and $\Delta\sigma \approx \partial_T\sigma|_c \Delta T + \partial_c\sigma|_T \Delta c$.

Another way for the system to get out of equilibrium are density differences $\Delta\rho$ to which the gravitational acceleration g couples, implying a

- **Rayleigh number** $Ra = gR^3\Delta\rho/(\rho\nu D)$, which compares destabilizing buoyancy with stabilizing viscosity and diffusivity.

Once chemical reaction come into play, we will also need the

- **Damköhler number Da**, which expresses the ratio between chemical reaction rate and (diffusive or convective) mass transport rate.

We will encounter all these numbers in the discussions of the various physicochemical hydrodynamical effects featured in this review article.

Box 2: Recent progress in experimental tools to address physicochemical hydrodynamics

A whole plethora of new and improved experimental techniques in fluid dynamics has enabled the recent progress in understanding the physicochemical hydrodynamics of droplets and bubbles far from equilibrium. The most relevant of these techniques are:

- **Optical visualization** with optical wavelength resolution and beyond: These techniques include standard, fluorescence, and confocal microscopy [15–17]. The latter allows for 3D visualizations, but the choice of proper dyes is essential, as adding dyes and/or fluorescent molecules (which are often surface active substances) may cause contamination to the system and artefacts.

- **Digital Holographic Microscopy (DHM)** can be seen as complementary to confocal microscopy, namely focusing on *interfaces* rather than on the bulk as standard confocal microscopy. The technique – developed only about a decade ago and up to now mainly used in the biological context [18–20] – is crucial and ideal for high-precision measurements and visualizations of growing and shrinking droplets with small contact angle, having a sub-nanometer *in-depth* resolution.

- **Micro-particle-image-velocimetry (μ-PIV)** [21] allows to obtain information on the velocity fields in and around droplets, even if they are moving, growing, or shrinking.

- **High-speed imaging** with frame rates up to several million frames per second [22] and **stroboscopic illumination** by nanosecond laser pulses [23, 24] allow for excellent temporal resolution. These techniques also include fluorescent high-speed imaging [22].

- **Atomic force microscopy (AFM)** allows for nanometer or even atomic resolution both laterally and in-depth. In the last two decades, it has developed such that it can now routinely also be used in the liquid phase [11]. With techniques like shock-freezing [25] or instantaneous polymerization with the help of UV radiation [26] the nucleation and growth process of droplets can be terminated. The latter requires the use of UV polymerisable liquids as solutes. After solidification of the sessile droplet phase through UV radiation, the other liquid phase can be removed, paving the way for AFM of a solid phase in air, which is much easier than of a liquid phase in another liquid.

- **Surface-enhanced Raman spectroscopy (SERS)** [27] allows to follow the chemical composition of sessile droplets or bubbles in time.

- **Microfluidics:** Well-defined channels and substrates with designed structures and chemical patterns are possible by microfabrication techniques [28–33] to study the growth and collective interactions of bubbles and droplets.

Box 3: Recent progress in numerical tools to address physicochemical hydrodynamics

Alongside the progress in the experimental techniques (see Box 2), also the progress on the numerical side was crucial in pushing the field ahead. Next to the ever enhancing pure computational power, also the development of new numerical methods and open-source codes and tools contributed to this progress, which now often make a one-to-one comparison between experiment and numerical simulations possible.

The main challenge for the numerical simulations in physicochemical hydrodynamics are the vastly different time scales for the momentum transfer and for the mass transfer, reflected in the large Schmidt number $Sc \approx 10^3$. This implies that the concentration field must live on a smaller grid than the velocity field and that the stepping time scale is extremely small. Here, multigrid resolution techniques are a possible way out [34]. These can be used for various numerical schemes.

The most relevant techniques for the numerical simulations in physicochemical hydrodynamics are:

- **Finite element methods:** Moving droplets or droplets with mass-exchange require a well-resolved interface with the surrounding phases. This can be achieved with a sharp-interface finite element method, where the mesh is always conforming with the interface [35]. Since in general the droplet moves, this requires to co-move all mesh nodes accordingly with the interface. To that end, with Eulerian-Lagrangian methods originally developed for fluid-structure interaction [36, 37], the mesh can be treated as pseudo-elastic body, so that the bulk nodes follow the motion of the interfacial nodes, which is connected via Lagrange multipliers to the kinematic boundary condition of the interface [35]. This technique has proven to be extremely versatile for binary and ternary droplets [17, 38–40], but the challenge remains to efficiently parallelize such codes.

- **Finite Difference (FD) with Immersed Boundary methods (IBM)** [34, 41] are an alternative, allowing for massive parallelization and the calculation of tens of dissolving or growing droplets over a long time [42, 43]. Just as in finite element methods, a weak point of such simulations is that they require *a-priori* input in what mode (e.g. constant contact angle (CA-mode) vs constant contact radius (CR-mode) [8, 11]) droplets or bubbles grow or shrink.

- **Phase field methods and Cahn-Hilliard type approaches** [44] employ a diffuse interface, but easily allow to describe spontaneous phase-separation and nucleation, such as occurring in the ouzo effect [45].

- **Level-set methods** [46, 47] have the advantage that the interfaces between the different phases are sharp. They have been extended to include phase changes and interfacial flows driven by surface tension gradients [48, 49].

- **Lattice Boltzmann (LB) methods** [50] – coarse-grained versions of the molecular theory of fluids enabling massive parallelization – have been adopted and applied to multiphase flows [51, 52], including the selective evaporation or dissolution of multicomponent droplets [53].

- **Molecular Dynamics (MD) simulations** [54–57] have the advantage that they do not require to predetermine whether the (sessile) droplet grows or shrinks in the CA or CR mode as in FD+IBM, but the mode will come up from the respective chemical properties of the substrate and the liquids involved, see e.g. refs. [58, 59]. The downsides of MD are that (i) only small nanodroplets (∼50 nm) can be simulated, that (ii) one is restricted to short physical times of at most microseconds, and that (iii) molecular interaction potentials are needed, which are not from first principles.

2 Recent fundamental research on physicochemical hydrodynamics in droplet systems

In this section we will give examples for the physicochemical hydrodynamics in selected simple droplet systems. We will focus on systems in which modern experimental and numerical techniques have led to considerable progress in our understanding, often even allowing for a one-to-one comparison between experiments and numerics. These modern techniques are highlighted in boxes 2 (experimental) and 3 (computational). In the next section we will focus on the applications and the relevance of these examples. The focus is on droplets – for a very general overview on fundamental and applied aspect of bubble systems, we refer to our recent review [60].

2.1 Immiscible droplet in a concentration gradient

One of the most basic examples for a droplet far from physicochemical equilibrium is the one of an immiscible (oil) droplet (of radius R) in a concentration gradient of two other miscible liquids (with density lighter respectively heavier than the oil droplet), see figure 1a. The two control parameters reflecting the non-equilibrium situation are the Marangoni number Ma defined with the gradient of the surface tension, i.e., $\Delta\sigma = R\partial_z\sigma$, and the Rayleigh number Ra, defined with the gradient in density, $\Delta\rho = R\partial_z\rho$; see box 1 for the proper nondimensionalization. For the case of Stokes flow (small Reynolds number) and zero density gradient, the resulting velocity and the concentration fields can be analytically calculated [61]. The former can be quantified by the Marangoni velocity V_M at the equator of the droplet or, in dimensionless form, the (Marangoni-)Peclet number $Pe_M = V_M R/D$. If large enough, i.e., for a large enough concentration gradient, this Marangoni flow can make the droplet jump upwards in the stratified density gradient, against gravity [39]!

In more detail, what happens is the following series of events, that we will describe for the concrete example of an anise oil droplet in a stratified (fully miscible) mixture of water (bottom) and ethanol (top) with constant density gradient in between, see figure 1a,b,c and ref. [39]: First, the oil droplet sinks in the gradient region, trying to find its equilibrium position with respect to density. Ethanol-rich liquid is entrained downwards during this motion. This entrainment is enhanced by the Marangoni flow along the drop surface, from the ethanol-rich top (low surface tension) to the ethanol-poor bottom, leading to further entrainment of ethanol-rich liquid. As the droplet asymptotically approaches the density matched position, the self-enhancing Marangoni flow eventually overcomes the sinking-induced buoyancy jet. This positive feed-back leads to a linear instability and exponential growth of the Marangoni flow, which pushes the liquid around the drop downwards and thus the drop upwards, like a micro-swimmer in the pulling mode [3]. Once this Marangoni flow is dominant (typically after $\sim 60s$), the drop shoots upwards towards the low density region and the process can start over. Up to six hours of consecutive jumps have been observed. The process only comes to an end once the jumping droplet has sufficiently mixed the stratified liquid. The system can be seen as canonical example for the competition between Marangoni (surface tension forces) and Rayleigh (gravity). We will see further examples in other subsections.

In general, the velocity U of a droplet in a concentration gradient is described with its so-called mobility M, namely $U = M\nabla c$, with the mobility being determined by the droplet radius R, the concentration dependence of the surface tension, and the dynamic viscosities $\eta_{i,o}$ of the inner and outer liquid, $M = R\partial_c\sigma/(2\eta_o + 3\eta_i)$ [61, 66–68], provided no other phoretic forces play a role.

Flow driven by concentration gradients and restricted to a few nanometers close to a *solid* interface is called *diffusiophoresis* [66, 67, 69, 70]. This term in particular refers to the motion of a colloidal particle in a concentration gradient. Though both Marangoni flow and diffusiophoresis originate from the interplay of surfaces with compositional gradients, we will not focus on diffusiophoresis in this review, as in general the term refers to liquid-solid interfaces, and not to droplets. Note however that there are some exceptions; e.g. in refs. [71, 72] the movement of a charged oil

droplet in a solute gradient is referred to as diffusiophoresis, as then a discontinuity in the flow velocity across the droplet interface arises, while the hydrodynamic stresses at the interface are continuous, see figure 1 of ref. [72].

2.2 Coalescence of droplets of different liquids

A concentration gradient can instantaneously be imposed by a collision of two droplets consisting of two different liquids. In the case of coalescence of fully miscible droplets, the surface tension difference at the interface will lead to Marangoni flow, with the droplet of smaller surface tension being pulled over that with the larger one, while the counteracting force in general is of viscous nature. The droplets can either be sessile [73, 74, 78] or pendant [75] from a nozzle with a large contact angle, or even hitting each other in flight [76, 79], or – both as sessile droplets – sitting on top of each other [77], see figure 2.

Note that the droplets need not be of equal volume and that the coalescence of a droplet with a pool of a different liquid is included in case (b) of figure 2. In that case, for large enough Ohnesorge and Marangoni numbers (i.e., dominance of Marangoni forces), the spreading front $L(t)$ displays a universal scaling law $L(t) \sim t^{3/4}(\Delta\sigma)^{1/2}/(\rho\eta)^{1/4}$ or $L(t)/R \sim (Ma/Sc)^{1/2}\ (t\nu/R^2)^{3/4}$ (where R is the droplet radius) over many orders of magnitude [75, 80, 81]. For case (a) of figure 2 – sessile droplets – the dynamics can be much richer, as, depending on the surface tension difference $\Delta\sigma$, it can either show enhanced coalescence similar to the case in figure 2b , or, more remarkably, *delayed* coalescence, due to a competition between capillary pressure and dynamic pressure, induced by the Marangoni flow, see figure 2a.

The situation further complicates once the different liquids in the drops react with each other [82] or a solidification (e.g. with cross-linkers) is induced [76], see sketch of figure 2c. Then the crucial new parameter is the Damköhler number, which compares the time scale of the chemical reaction with that of the hydrodynamics. Yet another situation occurs when one larger sessile droplet is immersing a smaller one of a different liquid, as shown in figure 2d. When the two three-phase-contact-lines touch each other, for certain combinations of surface tensions part of the interior sessile droplet can be "spit out" by the larger one [77], see figure 2d.

2.3 Droplets in concentration gradients emerging from chemical reactions

In the examples of the two previous subsections the concentration gradient leading to Marangoni flow was imposed from outside. However, such a gradient can also evolve, e.g. thanks to chemical reactions. A famous example for such gradients can be achieved with so-called Janus particles, i.e., particles with different chemical composition on different sides [83]. In the particular work of Paxton *et al.* [83] one side of the Janus particle consisted of gold and the other one of platinum. When put in a H_2O_2 solution, on the Pt side catalytically generated oxygen nanobubbles emerged, leading to a chemical potential gradient, which induced a (generalized) Marangoni flow along the particle surface, pushing the particle backwards. There are many variations of such systems, employing the concentration gradient between front and rear, e.g. in refs. [84–87]. Note that only very small gradients $\nabla\sigma$ in surface tension are required to drive visible motion of the microparticles [4].

For Janus particles, the symmetry-breaking is imposed on the particle. However, even more interestingly, such symmetry breaking leading to a gradient in concentration around a particle or droplet can also emerge *spontaneously*, due to an instability. Michelin *et al.* [63] theoretically showed that for large enough Peclet numbers the combined effect of solute dissolution (solubilization) (or solute reaction) at the droplet interface and Marangoni flow can produce an instability, resulting in spontaneous and self-sustained motion of the initially isotropic droplet [68, 88–91]. Here the Peclet number is defined with the mobility M of the droplet, the surface emission rate α [84], and the droplet radius R, namely $Pe = M\alpha R^2/D^2$. The crucial mechanism is that nonlinear mixing of the dissolved substance or the reagent establishes gradients in concentration, which

then are converted into flow by Marangoni forces or diffusiophoresis [66, 92–95]. The bifurcation diagram of this process and the resulting swimming velocities are shown in figure 1e, along with the concentration fields around the droplets for various Peclet numbers, see insets of figure 1e. They and figure 1a also give an idea on the flow field around the swimming droplet. For even larger Peclet numbers, the droplet can curl [64], swim helically [96] or even chaotically [65, 68, 72]; examples are shown in figure 1f,g. Once two or even more of such droplets are close to each other, they show very rich and highly nontrivial collective behavior [97–100].

The solubilization or chemical reactions at the droplet interface can be of various nature. Many examples are given in the review article by Maass *et al.* [4]. These include simply dissolving or slowly reacting droplets, but also micellar solubilization [101, 102] of a surfactant on the oil droplet well above the critical micelle concentration (CMC), nematic liquid crystal droplets self-propelling in a highly concentrated surfactant solution [64, 96, 103], droplets with a surfactant undergoing a chemical reaction [97], binary droplets with selective dissolution [104], and many others [4]. Obviously, the driving strength of solubilization or dissolution will decrease as function of time and the droplet will shrink, leading to transitions in the motion pattern, e.g. from random, to helical, to straight [96], but this process is very slow and can take many hours. An interesting case is also when the droplet crosses its own trace. Another flabbergasting case is a surface-active chemotactic droplet which is even able to navigate through a complex maze, thanks to an imposed concentration gradient and the self-propelling property [62, 105, 106]. Such an example is shown in figure 1d.

2.4 Droplets in concentration gradients emerging from phase transitions

The simplest case of a droplet in an out-of-equilibrium situation may be a volatile droplet evaporating in air or a soluble droplet dissolving in another, originally pure liquid. For a spherical droplet in the *bulk* of a host liquid this problem was analytically solved by Epstein and Plesset [107]. That calculation was originally made for dissolving bubbles, but later generalized to dissolving droplets [108]. Also the evaporation or dissolution of a single *sessile* droplet consisting of a pure liquid in a solvent has meanwhile reasonably well been understood [8, 9, 11, 109–114] – even if it is not purely diffusive so that convective effects outside the droplet due to density differences of the liquids come into play [115], enhancing the dissolution.

The situation becomes more interesting once *multiple* dissolving or evaporating sessile droplets interact, as in general they shield each other: The reason is that dissolving neighboring droplets reduce the concentration gradient at the interface and thus the outflux from the droplet, leading to longer (and heterogeneous – depending on the position of the droplet) life-times [42, 43, 116–120], even when the solvent is flowing over the sessile droplets [42]. Such a situation has recently been explored both experimentally and numerically, leading to reasonable agreement, as seen in figure 3. Note that the dissolution delay by shielding only holds in the pure diffusive regime. Once convective effects come into play (i.e., density difference between the droplet and its host liquid with large resulting Rayleigh numbers), remarkably, collective effects can also *enhance* dissolution, due to the collective interaction of individual density plumes [120].

Coming back to single sessile droplets, concentration gradients can also emerge from selective evaporation (or dissolution) from a sessile *binary* droplet (or – again more generally – a droplet consisting of several miscible liquids). The reason lies in a combination of the (in general) different volatility of the components and the singularity of the evaporation (or dissolution) rate at the rim of the droplet [8, 110, 112, 121] (provided the contact angle is smaller than 90^o), leading to a concentration gradient at the interface of the droplet. The resulting surface tension gradient drives a Marangoni flow inside the droplet [17, 38, 40, 122–132], see figure 4a. This effect is very similar to what leads to the so-called tears of wine [133] inside a partially filled wine-glass: In this case, selective evaporation of ethanol at the edge of the meniscus leads to larger surface tension, which thus pulls part of the remaining wine upwards along the alcohol-wetting glass, finally leading to an instability of the film and droplets sinking down the glass wall. In evaporating droplets, the

Marangoni convection can be so violent – with velocity exceeding mm/s – that the axisymmetry breaks [38, 125]. The same can happen through moisture absorption: Shin *et al.* [134] show that the absorption of water vapor (i.e., moisture) to a sessile or pendent glycerol droplet can lead to an axisymmetry breaking Bénard-Marangoni instability of the resulting flow, which is driven by water concentration gradients at the droplet-air interface, emerging from preferential absorption of the water at the rim of the droplet. The evaporation, absorption, and dissolution dynamics of multicomponent sessile droplets presently is a very active area of research.

Depending on the nature of the two components of the binary liquid, the (stronger) evaporation of one component can lead to several different scenarios for the physicochemical hydrodynamics of the sessile binary droplet. In a first scenario [129, 130, 135], the selective evaporation of one liquid can lead to segregation of this liquid in the center of the droplet thanks to shielding by the other, non-volatile liquid. This scenario occurs once the Marangoni flow arising through concentration differences at the droplet-air interface is too weak to fully mix the two liquids.

An even more interesting second scenario comes into play once the two miscible liquids of the binary droplet display a sufficiently large density gradient [40, 131], as can become the case for e.g. a droplet consisting of water and glycerol [40]. This density gradient is "activated" by selective evaporation of the more volatile liquid, which in ref. [40] is water. In dimensionless form, it is expressed as Rayleigh number Ra. The gravitational forces resulting from the density gradient compete with the Marangoni forces on the droplet-air interface, whose strength in dimensionless form is expressed as Marangoni number Ma. Once the gravitational forces win, Rayleigh convection rolls dominate and the flow pattern in sessile droplets (figure 4b) is very different from that in pendant droplets (figure 4c). For sub-millimeter droplets this is remarkable as the Bond number of such droplets is $Bo \ll 1$, on first sight implying that gravity does not play a role – but only as compared to capillarity (implying the spherical-cap-shape of the droplet), but not as compared to viscosity. The full phase diagram in the Ra vs Ma parameter space is displayed in figure 4d, featuring either pure Rayleigh convection rolls, or pure Marangoni convection rolls, or both at the same time. Also for large Rayleigh numbers the axisymmetry can be broken, and a Rayleigh-Taylor instability can emerge [137].

Instabilities can also emerge once a binary droplet evaporates on a bath of an immiscible liquid [81, 138, 139], see figure 5a. Here, similarly as in subsection 2.2, the Marangoni stress in the drop pulls the droplet outwards but is balanced by the viscous stress in the oil bath, leading to a bulk flow (black arrows in figure 5a1). The evaporation causes a transition from partial to complete wetting, which sets the radius of the central drop in figures 5a2,a3. In the limiting case of the bath height going to zero, one has the situation of a binary droplet on a thin film. Here the outwards Marangoni flow can get so violent that a hole emerges in the film [140].

The dynamics of an evaporating binary sessile droplet – be it on a substrate or a liquid – is further complicated once also surfactants come into play [125, 128]. Also in this case the Marangoni driving of the flow can be so strong that its axisymmetry is broken. The surfactants and the composition of the binary droplet also strongly affect the pattern of the deposit as Kim *et al.* demonstrated with evaporating whisky droplets [125].

Note that not only the dissolution of sessile binary droplets with the resulting Marangoni flows is highly non-trivial, as elaborated above, but even the dissolution of spherical binary droplets in the bulk: The reason is that, due to selective dissolution, concentration gradients inside the droplet between its surface and its bulk can arise [144]. These can lead to considerable memory effects (in particular for small droplets), which do not exist for the dissolution of a pure droplet [144–146].

Another example for a concentration gradient (i.e., an out-of-equilibrium situation) which emerges from phase transitions is a freezing miscible mixture of different liquids with different freezing temperatures. A particularly intriguing case is a pure immiscible droplet in a binary liquid undergoing solidification of one component [147]. Then a concentration gradient is emerging, acting on the droplet, either pushing it away from the solidification front or towards it, possibly finally

leading to the engulfment of the droplet [141]. An example is shown in figure 5b. A generalization of this problem are freezing colloids which show extremely rich and intriguing behavior [147].

2.5 Droplets in ternary liquids: Nucleation and growth

The examples up to now dealt with miscible, sparingly miscible, and immiscible liquids, but the solubility of one liquid in another one was always constant. However, in ternary liquids, this need not be the case: The mutual solubilities in general depend on the relative concentrations of the liquid. This is commonly expressed in the so-called ternary diagram, see figure 6a for a sketch of a typical situation. In particular, the ternary diagram can contain so-called ouzo-regions, in which sub-micrometer-sized droplets of one species can metastably exists. The best-known example for such liquids is indeed ouzo itself.

Ouzo is a transparent Greek liquor (equivalently, one can take as example the French Pastis, the Italian Sambuca, or the Turkish Raki), which chemically – in spite of its actual more complex composition – for our purposes can be considered as a ternary liquid consisting of ethanol, water, and (anise) oil. When served, water is usually added, which lowers the solubility of the oil (see the ternary diagram of figure 6a), thus leading to oil oversaturation and subsequently to the nucleation of oil droplets in the bulk liquid and thus to the characteristic milky color. This process is called "ouzo effect" [148–150] or also *solvent exchange* or *solvent shifting*. The ouzo emulsion is amazingly stable against Ostwald ripening [151, 152], i.e., the capillary pressure driven shrinkage of the smaller droplets and the simultaneous growth of the larger ones (coarsening). Moreover, the nucleated droplets have a relatively sharp size distribution. Both features – the absence Ostwald ripening and the sharp droplet size distribution – are not fully understood and an active area of research [153].

When the solvent exchange process takes place in the presence of a hydrophobic surface, *sessile* nanodroplets will nucleate at this surface and then grow [11, 26]. This offers the opportunity for a *bottom-up approach* in "building" droplets or also crystals. Nucleation and growth of the droplets strongly depend on the geometrical and chemical nature of the substrate and pinning of the contact line respective the absence thereof plays a paramount role [154, 155] in determining the growth mode of the droplet (constant contact radius (CR) mode vs constant contact angle (CA) mode). It is this pinning that enables the stability of surface nanodroplets and nanobubbles against evaporation or dissolution [11, 156, 157].

The advances in modern microfluidics and microscopy of various kinds (see box 2) allowed to monitor the growth of the nucleated sessile nanodroplets as function of the control parameters [163, 164, 168, 169] – including on patterned surfaces [170, 171], as function of time [172], and including collective effects of the nucleating droplets [173–175].

The essence of the process is sketched in figure 6b: A bad (but fully saturated with a solute) solvent in a narrow channel (of submillimeter height h) is replacing a good one (also saturated or at least containing sufficient solute), leading to a front of oversaturation of the solute, which passes by the substrate. This passage leads to nucleation of nanodroplets on the substrate (provided the wetability of the droplet liquid on the substrate allows for this) and to their growth. This growth is controlled by the thickness of the diffusive boundary layer around the droplets (which is set by the Prandtl-Blasius-Pohlhausen boundary layer theory [176]) and thus the mean flow velocity, or, in dimensionless numbers, the Peclet number Pe. One can theoretically derive $\langle Vol_f \rangle \sim h^3 Pe^{3/4}$ for the final area averaged volume $\langle Vol_f \rangle$ of the droplets [163, 177], which agrees very well with the experimental data.

The solvent shifting can also be driven by evaporation or dissolution of one of the solvents. Such experiments combine features of the Marangoni flow in ternary droplets triggered by evaporation or dissolution as described in subsection 2.4 with the nucleation of microdroplets triggered by solvent shifting as described in this subsection.

A very illustrative and simple example for such an experiment is the evaporation of an ouzo droplet on a substrate under ambient conditions [17, 38], see figure 7, where we show optical and

confocal snapshots and sketches of the four different stages of the evaporation process of the ouzo droplet [17, 38]: In phase I, the spherical cap-shaped droplet remains transparent, while the more volatile ethanol is evaporating, preferentially at the rim of the drop due to the geometric singularity there, as explained in subsection 2.4. This leads to a local ethanol concentration reduction and according to the ternary diagram figure 6a to oil droplet nucleation at the rim. This is the beginning of phase II, in which oil microdroplets quickly nucleate in the whole drop, leading to the typical milky ouzo appearance. These microdroplets can coalesce and form an oil ring at the rim of the droplet (early in phase III). At some point all ethanol has evaporated and the drop, which now has a characteristic non-spherical-cap shape with the water drop sitting on top of the oil ring, thus is transparent again (late in phase III). Finally, in phase IV, also all water has evaporated, leaving behind a tiny spherical cap-shaped oil drop. The entire evaporation process takes about a quarter of an hour. Note that this example of an evaporating ouzo droplet on a substrate can also numerically be treated, employing finite element methods, resulting in a very good agreement between numerics and experiments [17, 38].

There are various variations of the theme of an evaporating or dissolving ternary droplet: In ref. [178] an ouzo droplet evaporating on a superamphiphobic surface is studied, again both experimentally and numerically. In this case the contact angle is much larger than 90^o, resulting in a maximal evaporation rate at the apex of the droplet and correspondingly to a start of the oil microdroplet nucleation at that position. Obviously, the Marangoni flow is then also towards the apex of the droplet, and not towards the rim, as it was the case for contact angles smaller than 90^o. In ref. [179] the dissolution of a water-ethanol drop in a bath of anise oil was analyzed: Here during the dissolution, two types of microdroplet nucleation was observed, namely oil microdroplet nucleation in the aqueous drop ("ouzo effect") and water microdroplet nucleation in the surrounding oil ("inverse ouzo effect"), see figure 6a. Again, various physicochemical hydrodynamical processes such as Marangoni flow, Rayleigh convection, diffusion and nucleation compete in an extremely rich way, but can nonetheless be disentangled [179] by including the key physics in a simple model [179–182].

An even richer system with two big drops consisting of different aqueous liquids (one water drop, and one consisting of ethanol-water mixtures) in a bath of toluene as host liquid is studied in ref. [183]. The diffusion of the aqueous liquids through the toluene leads to the nucleation of aqueous microdroplets (inverse ouzo effect) in between the two bigger drops. A variation of this experiment is sketched in figure 6c1: Two droplets of two different slightly soluble liquids are approached to each other in a third liquid. Even before they touch (a situation we had discribed in subsection 2.2), there will be diffusive exchange of matter. In figure 5c the solubility of the yellow liquid is larger than that of the red one, leading to a concentration gradient of the yellow liquid on the red drop and thus in general to Marangoni forces and the resulting Marangoni flow in the red drop and in between the drops. This will dramatically change the diffusive process and the forces between the droplets. In case of ternary liquids with a solubility gap it can also lead to nucleation of microdroplets, as in ref. [183].

Droplets of ternary liquids can phase separate in many different ways [45, 153, 159, 167, 184–186], showing extremely rich and complex behavior. For example, a miscible droplet of diethylphthalate (DEP) oil, water, and ethanol, which has a ternary diagram similar to that shown in the sketch of figure 6a, demixes upon contact with an aqueous phase, to give alternating, onion-like layers of oil and water [45, 167], see figure 6c. The detailed dynamics of this liquid-liquid phase separation and the type of emerging structures strongly depends on the exact relative initial composition of the ternary liquid and their viscosity. The process is controlled by diffusion of water into the ternary droplet and vice versa of its components out of the droplet. The liquid-liquid phase separation can be modelled with Cahn-Hilliard type approaches [45].

A microfluidics co-flow device similar to that of figure 6c1 operated with ternary liquids is also very well suited to impose a well-defined concentration gradient, in order to quantitatively study the competition between diffusion, Marangoni convection, and nucleation of microdroplets

in the ouzo-region or inverse ouzo-regime of the ternary diagram [187]. The reason is that, with the controlled and laminar flow profiles of such a device, detailed experimental information on the conditions for droplet formation and their radial migration in the ternary flow can be obtained and compared with the ternary phase diagrams.

3 Relevance and applications of physicochemical hydrodynamics in droplet systems

After having shown some examples of recent fundamental work on the physicochemical hydrodynamics in well-defined droplet systems in the previous section, we will now come to the relevance of multicomponent droplet systems in applications. In the introduction we have already mentioned various application fields. In the following subsections we want to go into more detail for five quite different application fields. Also for these applications we cannot be encyclopedic, nor go into depth, but we hope to convey the flavor of the applications and their great potential. As in the previous section we ended with ternary droplets with a solubility gap, here we will directly continue with them, and only then come to miscible binary and multicomponent droplets.

3.1 Chemical analysis and diagnostics

Liquid-liquid extraction – the transfer of a solute from one solvent to another – is one of the core processes in chemical technology and analysis. For chemical analysis such as chromatography, ever since the pioneering work of the Nobel Laureate Fritz Pregl [142] on microanalysis, there have been continuous efforts to further miniaturize the extraction process of the analyte and to optimize the extraction recovery and preconcentration factor. The driving factors for the miniaturization have continued to increase in recent years [12], reflecting the urgency of the problem: First, the need to detect *trace quantities* of some substance is still increasing in the medical, biomedical, food safety, and environmental context. Next, the health monitoring systems of the future will be based on *rapid* measurements on *small* sample volumes. Finally, the miniaturization will lead to less chemical waste and environmental strain, i.e., towards "greener" analytical methods and process technologies.

In the last two decades so-called *single-drop microextraction* [12] has become very popular for sample preparation of trace organic and inorganic analysis. The principle of this method is shown in figure 5d. Here a solute A dissolved in water accumulates in a droplet of water-immiscible liquid B, due to its higher solubility in B as compared to water. After an equilibrium has been achieved, the droplet, which now consists of a mixture of A and B, is extracted with a syringe, to be further analysed by e.g. chromatography.

The scale on which single-drop microextraction can be done obviously remains limited, but this limitation is overcome in the modern technique of *dispersive liquid-liquid microextraction* (DLLME), which was invented less than 15 years ago [143, 188, 189] and heavily makes use of the solubility gap of ternary liquids and thus the ouzo effect as explained in subsection 2.5. Here, a mixture of two miscible liquids B and C (with low concentration of B) is put into water containing the analyte A, with B being immiscible with water (say, carbon-tetrachloride [189]), but C being miscible (say, acetone [189]), see figure 5e. When poured into the aqueous solution containing A, droplets of B will immediately nucleate and then further grow out of the oversaturated solution. The liquid B is chosen such that it has much higher solubility for the analyte A than water and is heavier than water and liquid C. The large total surface of the nucleated microdroplet ensemble will greatly help the extraction process. The final step is to centrifuge the dispersion and take out the A-B phase.

The relevant parameters to characterize the performance of liquid-liquid extraction processes are the so-called preconcentration factor, defined as the ratio of the analyte concentration in the centrifuged droplets, and the so-called extraction recovery, defined as the percentage of analyte

which could be extracted. Hitherto, it has not been possible to *a-priori calculate* these parameters, hindering the optimalization of liquid-liquid extraction processes, which presently is often done by trial-and-error. Even liquid-handling robot systems [190] were built to automate the evolutionary process of finding the optimum. Clearly, a quantitative understanding of the nucleation and the diffusive dynamics of droplets in ternary systems is crucial to make progress towards a quantitative understanding and systematic optimization of DDLME.

Another diagnostic application of the physicochemical hydrodynamics of droplets far from equilibrium is nanoextraction of tracers [191]. Sample preparation is considered to be the most difficult step in analytic workflow. Current methods for extraction and separation of minute amounts of substances in liquid samples are laborious, time-consuming, often involve large amounts of toxic organic solvents, and are difficult to automatize, implying high costs of man-power. However, liquid-liquid extraction and online analysis of traces of analytes in aqueous solutions, including in biomedical, health, pharmaceutical and environmental contexts, may be dramatically improved by surface nanodroplet-based sensing techniques [192–194]. The basis of such nanoextraction are surface nanodroplets pre-formed by solvent exchange on a substrate within a microflow channel. The principle is that the partition coefficient of the compound in the droplets is much higher than in the solution. The compound in the liquid can thus be extracted into the surface nanodroplets and be quantified by surface-sensitive spectroscopic techniques [194]. This approach can potentially achieve extraction-detection of analytes at extremely low concentrations in one single and simple step, allowing for fully automized sample analysis through programmable nanodroplet production for extraction and in-situ detection.

3.2 Pharmaceutics and chemical & environmental engineering

The ouzo effect is not only relevant for microextraction in chemical analysis and diagnosis, but also for drug production and delivery [150] and in pharmaceutical science and cosmetics [195], providing a basis for the preparation of pharmaceutical products, formulation of cosmetics and insecticides, liquid-liquid extraction and for many other practical processes. In this context the ouzo effect is also called "nano-precipitation". Small hydrophobic organic molecules, lipids, or polymers also exhibit similar microphase separation and, by mixing them with a poor solvent, form nanodroplets or nanoparticles with homogeneous sizes. Note that often the details of the mixing process matter. Why this is the case has not yet been fully understood. E.g., in some case the mixing must be very rapid – a process then called "flash nanoprecipitation", which has been demonstrated to be a simple way to produce drug-loaded polymeric nanoparticles, protein nanoparticles, and other multifunctional colloids with narrow size distribution [196–198]. Droplet formation by solvent exchange is also highly relevant for separation and purification in other applications of the chemical and pharmaceutical industry, including undesirable oiling-out crystallization in production of pharmaceutical ingredients, amino acids, and proteins [199].

Also on a larger scale, understanding and controlling nucleating and growing droplets in liquid-liquid phase separation is essential for improving the efficiency of industrial operations, e.g. in extraction of natural resources, recycling of valuables from waste and removing organics in waste water treatment, in flotation, and in renewable energy technologies.

Finally, dilution-induced phase separation (i.e., the ouzo effect) is important for advanced oil recovery processes [200]. An example is paraffinic froth treatment in the industrial process of oil sands extraction [201]. Heavy oil bitumen with a considerable amount of fine solids and water is separated from oil sands ore by warm-water extraction to form bitumen froth. Solids and water are removed by adding sufficient light alkane (which is a poor solvent for asphaltenes, a solubility family of extremely heavy species of bitumen) to achieve a critical solvent/bitumen ratio. Asphaltene precipitation triggered by this dilution then forms agglomeration with water drops and solids, sweeping the solids and water off under gravity and producing diluted bitumen of high quality which is easy to transport [202]. Control of the size distribution and morphology of asphaltene precipitates may lead to a more efficient oil recovery approach, with less hydrocarbon

loss to waste [200].

3.3 Synthetic chemistry and biology

Apart from encapsulation and precursors for nanoparticles as described in the previous subsection, the droplets and their physicochemical hydrodynamics also find many applications in chemical synthesis. They provide a confined environment in synthetic chemistry to realize cascade reactions in a fashion similar to artificial cells. The surface of microdroplets serves as a biphasic site for catalysts to access immiscible liquid phases inside and outside of droplets, significantly improving the specificity and efficiency of interfacial catalytic reactions for biofuel upgrading [203]. The droplets generated from chemical reactions were found to preferentially and differentially segregate and compartmentalize RNA, suggesting that droplets may play a role in protecting essential chemical components for the origin of life [204]. Indeed, the droplets can grow and divide from addition of materials produced in droplet reaction, resembling prebiotic protocells [205–207].

Microdroplets can also act as microlabs or chemical microreactors, and often chemical reactions, which do not take place in bulk water, do occur in microdroplets [208, 209]. To account for the enhanced chemical reactions in the microdroplets, a reaction-adsorption mechanism was proposed [210]. According to this mechanism, the molecules at the interface are more active, which is attributed to the solvation energy getting available thanks to solubilization. The energy required for the molecules at the interface to react is therefore less than that in the bulk reaction [210].

As an entity of microcompartment, droplets formed from aqueous liquid-liquid phase separation of polyelectrolytes have drawn intensive interest from biology and cell research. The process of phase separation of an aqueous solution consisting of two oppositely charged polyelectrolytes into two immiscible aqueous phases – coacervate droplets and supernatant – is called "coacervation" [211]. The dense coacervate droplets are rich in polymers while the supernatant is a dilute equilibrium phase, poor in polymers. Coacervation has a long history of utilization in encapsulation applications [212]. The process of coacervation was also proposed as crucial in theories of abiogenesis (the development of life) [213]. Coacervation is driven by both entropy and electrostatic interactions between polyelectrolytes, influenced by molecule weight, charge distribution and chirality of polymers, the concentration and the weight ratio of the two polymers and the ionic strength of the aqueous medium. Prior to the macroscopic phase separation, the size distribution of the polyelectrolyte complexes becomes very narrow. Intermolecular complexes of several hundred nanometers form until macroscopic phase separation occurs.

The research interest in this subject has recently further intensified due to the functional roles of intracellular coacervates and their relation to diseases [214], and due to the extraordinary properties of coacervates as new materials, namely underwater superglue, deep tissue bonding or bone fixation, scaffold coatings, bone cement, and drug encapsulating materials [215]. What remains largely unknown is the evolution of nanoscale coacervates. Model polyelectrolytes with defined molecular weight and charge distribution have been studied to understand the effect of charge patterns [216]. It would be interesting to quantify the temporal evolution of the coacervate nanocolloids during the phase separation process, to better understand its fluid dynamics.

3.4 Inkjet printing

Binary and multicomponent droplets obviously are extremely relevant in inkjet printing [217–220] as nearly all inks are multicomponent and not only contain pigments and surfactants, but also consist of various different liquids, with different surface tensions, volatilities, and viscosities. Moreover, different nozzles of an inkjet printer are operated with different inks. Both features imply that selective evaporation and coalescence of droplets of different liquids as described in subsections 2.4 and 2.2 are very crucial processes in inkjet printing.

This not only holds for droplets on the substrate towards which the droplets are jetted but also on the nozzle-plate of the inkjet channel, close to the nozzle out of which the droplets are jetted,

and to the meniscus of the ink itself. Here selective evaporation of one component of the ink can be a major problem, as we will demonstrate with two examples from piezoacoustic inkjet printing [217], which is one of the most advanced and most controlled forms of inkjet printing:

- In piezoacoustic inkjet printing, the ink in the nozzle is well mixed, thanks to the acoustic field driving the jetting of the droplets. Therefore the material properties of the ink such as surface tension or viscosity are determined by the composition of the various liquid components. Now imagine a nozzle at rest for some printing cycles, as that particular ink is not needed. In that time – say many seconds – one or more components of the ink can selectively evaporate out of the nozzle. This changes the material properties of the remaining ink such as the surface tension and therefore the required pulse strength for jetting once the nozzle is activated again – a major source of inaccuracy.

- Even worse, droplets of ink on the nozzle plate can selectively evaporate, introducing a concentration gradient and thus surface tension gradient on the nozzle, leading to a Marangoni flow [221, 222]. Once this flow is directed towards the nozzle it can lead to transport of dirt particle into the nozzle which can lead to air bubble entrainment and nozzle failure [223, 224] – a major disaster for the printing process.

Also on the substrate on which the droplets are jetted Marangoni flow within one droplet [17, 38, 40, 122, 125–132] (see figures 4a,b,c) or in between different droplets [73] (figure 2) can lead to unwanted effects, in particular as these flows transport pigments. Or does the emerging Marangoni flow between the droplets perhaps even help in mixing the droplets ("bleeding of mixed colors")? Yet another question is how the multicomponent nature of the evaporating droplet and the resulting flows affect the coating pattern [10, 125, 218, 225, 226]. The jetted multicomponent droplets on the substrate may in addition undergo phase changes by evaporation, solidification, or chemical reactions. In the latter case of *chemical reactions* inside the droplets, including reactions leading to *solidification*, as e.g. with crosslinkers [76], many questions arise: What does exactly happen when one reactant diffuses into a droplet of another reactant, e.g. from a neighboring droplet or from some reservoir? How does the reaction propagate from the droplet surface where the two reactants first make contact? How does a two-component paint "chemically dry" through crosslinkers? "Watching paint dry" is in fact interesting, relevant, and largely unexplored science! It is also very timely, because of sharpened environmental regulations with respect to the evaporation of (toxic) solvents.

3.5 Nanotechnology and nano- & micro-materials

The solidification process after drop-drop coalescence – with one droplet filled with crosslinkers and the other one with a liquid responsive to it – has indeed been used to manufacture microparticles of controlled shape and size at very high rate [76]. As the process takes place after collision of such droplets in air (see figure 2e), Visser *et al.* [76] called it "in-air microfluidics". Its control parameters are – next to the droplet sizes and their velocities – the droplet compositions, through which different degrees of Marangoni-flow-driven encapsulation can be achieved, leading to controlled mono-disperse emulsions, particles, and fibers with diameters of 20 to 300 μm.

Also ternary liquids have been used to manufacture micro- and even nanoparticles, namely by employing the ouzo effect – or then also called nano-precipitation. In fact, with this process micro and nanomaterials can be built bottom-up in a well-controlled way [227–229].

Another important material science application for which the physicochemical hydrodynamics of droplets is relevant are freezing colloids [147], as e.g. shown in figure 5b. Here the crucial question is: How do immersed droplets interact with the freezing front in binary or multicomponent freezing liquids? On the one hand particle-reinforced metal alloys require homogeneous distribution of particles in the matrix, and an immediate engulfment is therefore preferred. On the other hand, for single-crystal growth, a complete rejection of impurities is obviously crucial [141, 230]. A rejection

is also preferred whenever engulfed droplets or bubbles would introduce uncontrolled defects into a cooling alloy.

Finally, a very important application of the physicochemical hydrodynamics of droplets is in the semiconductor industry and in nanotechnology where surfaces like wafers have to be extremely clean and dry. This can be achieved by the so-called Marangoni drying [127, 231–235], where gradients in surface tension are imposed to drive the liquid of a thin film outwards, e.g. through local vapor deposition of a different fluid (often isopropyl alcohol – IPA), which absorbs on the film, or through deposition of a multicomponent droplet [140]. For Marangoni drying to work properly, the interaction of sessile droplets on the wafer is of course essential and unexpected hinderance of coalescence of droplets of different liquids as shown in refs. [73, 74] (see figure 2a2) are obviously a major problem.

In the context of drying wafers with their nanoscale structures, capillary forces can also cause major problems [236]: When a sessile droplet attached to different structures on a surface is evaporating, the capillary forces, which are tremendous on the tiny length scales relevant on wafers, pull these structures together, which can make them break [237–239].

4 General Lessons

We hope to have given an idea how in the last years the community is working towards a deepened quantitative understanding of physicochemical hydrodynamics of droplets far from equilibrium, in order to illuminate the fundamental fluid dynamics of immersed (multicomponent) (surface) droplets. To do so we have shown controlled experiments and numerical simulations for idealized setups, allowing for a one-to-one comparison between experiments and numerics/theory, in order to test the theoretical understanding.

Much remains to be done, both from a fundamental point of view, but also from the application side, with many new and extremely relevant applications of the physicochemical hydrodynamics of droplets far from equilibrium popping up at a very high rate. But we expect that the rapid progress in this field is continuing, as from our point of view we are living in the golden age of fluid dynamics: The reasons are the continuous increase in computational power, so that simulations which we did not dare to dream of even ten years ago are now possible and that a similar revolution (for the same reason) is taking place in digital high-speed imaging, thanks to which we can now routinely resolve the millisecond time scale and even smaller scales, revealing new physics on these scales, which up to now was inaccessible, and producing a huge amount of data on the flow. Moreover, other advanced equipment like confocal microscopy, digital holographic microscopy and atomic force microscopy are coming to be used more and more in fluid dynamics. Considering all of these advances together, the gap between what can be measured and what can be simulated *ab initio* is narrowing more quickly than we had anticipated at the end of the last century. Other gaps are also closing. Fluid dynamics is bridging out into various neighboring disciplines, such as chemistry, and in particular colloid science, chemical analysis and diagnostics, lab-on-a-chip mircrofluidics, catalysis, electrolysis, medicine, biology, computational and data science, among many others. Here the techniques, approaches and traditions from fluid dynamics can offer a great deal of help to solve outstanding problems. Vice versa, these fields can offer wonderful questions to fluid dynamics.

Finally, anyone who dismissed the experiments with tears of wine or with coffee, whisky or ouzo drops as a gimmick is very much mistaken: On the one hand, as we have seen, we learn important physics, chemistry, fluid dynamics, and colloid and materials science from these systems and processes, with many modern applications in diagnostics, pharmaceutics, biology, medicine, chemical and environmental engineering, inkjet printing, nanotechnology, and micro-manufacturing, all of huge relevance. On the other hand – and here we come to the education in science which may be even more important than one or the other application – the deciphering of these everyday phenomena are examples *par excellence* of the physicist's approach: first translate an observed

phenomenon into a clean experiment with well-defined control parameters, then make precise observations and record data, then develop a theory and a model and confirm these by calculations and numerical simulations, and finally make predictions about how the system will behave with values for the control parameters from an even wider range. Studying the fluid physics of these everyday systems is therefore also very suitable for the conceptual training of PhD students, who can learn in this way, simultaneously and by example, clean experimentation, theory formulation, modelling and numerical simulation, which from our point of view is much more motivating and broader than being a small cog for a specific detail of a large large-scale experiment with thousands of scientists involved.

Acknowledgements

We thank our colleagues, postdocs, Ph.D. students, and students for all their work and contributions to our understanding of physicochemical hydrodynamics of droplets and for the stimulation and intellectual pleasure we have enjoyed when doing physics together. In the context of the subjects covered in this review we would like to name Lei Bao, Kai Leong Chong, Pallav Kant, Ziyang Lu, Andrea Prosperetti, Vamsi Spandan, Michel Versluis, Claas-Willem Visser, Herman Wijshoff, Haitao Yu, and in particular Christian Diddens, Yanshen Li, Yaxing Li, and Huanshu Tan. Moreover, we thank Anne Juel, Stefan Karpitschka, Corinna Maas, Andrea Prosperetti, Jacco Snoeijer, and Howard Stone for comments on the manuscript. D.L. also acknowledges Dennis van Gils for drawing many figures and support from NWO under several projects, from the ERC-Advanced Grant "DDD" under the project number 740479, and from the ERC-Proof-of-Concept Grant "NanoEX" under the project number 862032. X.H.Z. acknowledges support from the Natural Science and Engineering Council of Canada (NSERC) and from the Canada Research Chairs program.

References

[1] V. G. Levich, *Physicochemical hydrodynamics* (Prentice Hall, Englewood Cliffs, 1962).

[2] M. E. Cates and E. Tjhung, *Theories of binary fluid mixtures: from phase-separation kinetics to active emulsions*, J. Fluid Mech. **836**, P1 (2018).

[3] E. Lauga and T. R. Powers, *The hydrodynamics of swimming microorganisms*, Reports on Progress in Physics **72**, 096601 (2009).

[4] C. C. Maass, C. Krüger, S. Herminghaus, and C. Bahr, *Swimming droplets*, Annu. Rev. Cond. Matter Phys. **7**, 171 (2016).

[5] J. L. Moran and J. D. Posner, *Phoretic self-propulsion*, Annu. Rev. Fluid Mech. **49**, 511 (2017).

[6] R. Golestanian, Phoretic Active Matter, arXiv: 1909.03747.

[7] H. Manikantan and T. M. Squires, *Surfactant dynamics: hidden variables controlling fluid flows*, J. Fluid Mech. **892**, P1 (2020).

[8] A. M. Cazabat and G. Guéna, *Evaporation of macroscopic sessile droplets*, Soft Matter **6**, 2591 (2010).

[9] H. Y. Erbil, *Evaporation of pure liquid sessile and spherical suspended drops: A review*, Adv. Colloid & interface Sci. **170**, 67 (2012).

[10] K. Sefiane, *Patterns from drying drops*, Adv. Colloid Interface Sci. **206**, 372 (2014).

[11] D. Lohse and X. Zhang, *Surface nanobubble and surface nanodroplets*, Rev. Mod. Phys. **87**, 981 (2015).

[12] A. Jain and K. K. Verma, *Recent advances in applications of single-drop microextraction: A review*, Analytica Chimica Acta **706**, 37 (2011).

[13] A. de Wit, *Chemo-Hydrodynamic Patterns and Instabilities*, Annu. Rev. Fluid Mech. **52**, 531 (2020).

[14] G. Vazquez, E. Alvarez, and J. M. Navaza, *Surface Tension of Alcohol Water + Water from 20 to 50 degrees C*, J. Chem. Eng. Data **40**, 611 (1995).

[15] S. W. Hell, *Microscopy and its focal switch*, Nature Methods **6**, 24 (2009).

[16] R. H. Webb, *Confocal optical microscopy*, Rep. on Progress in Phys. **59**, 427 (1996).

[17] H. Tan, C. Diddens, P. Lv, J. G. M. Kuerten, X. Zhang, and D. Lohse, *Evaporation-triggered microdroplet nucleation and the four life phases of an evaporating Ouzo drop*, Proc. Nat. Acad. Sci. **113**, 8642 (2016).

[18] P. Marquet, B. Rappaz, P. Magistretti, E. Cuche, Y. Emery, T. Colomb, and C. Depeursinge, *Digital holographic microscopy: a noninvasive contrast imaging technique allowing quantitative visualization of living cells with subwavelength axial accuracy*, Optics Lett. **30**, 468 (2005).

[19] J. Garcia-Sucerquia, W. Xu, S. Jericho, P. Klages, M. Jericho, and H. Kreuzer, *Digital in-line holographic microscopy*, Appl. Optics **45**, 836 (2006).

[20] F. Merola, L. Miccio, M. Paturzo, A. Finizio, S. Grilli, and P. Ferraro, *Driving and analysis of micro-objects by digital holographic microscope in microfluidics*, Optics Lett. **36**, 3079 (2011).

[21] S. T. Wereley and C. D. Meinhart, *Recent advances in micro-particle image velocimetry*, Annu. Rev. Fluid Mech. **42**, 557 (2010).

[22] M. Versluis, *High-speed imaging in fluids*, Exp. Fluids **54**, 1458 (2013).

[23] A. van der Bos, A. Zijlstra, E. Gelderblom, and M. Versluis, *iLIF: illumination by Laser-Induced Fluorescence for single flash imaging on a nanoseconds timescale*, Exp. in Fluids **51**, 1283 (2011).

[24] A. van der Bos, M.-J. van der Meulen, T. Driessen, M. van den Berg, H. Reinten, H. Wijshoff, M. Versluis, and D. Lohse, *Velocity Profile inside Piezoacoustic Inkjet Droplets in Flight: Comparison between Experiment and Numerical Simulation*, Phys. Rev. Appl. **1**, 014004 (2014).

[25] M. Switkes and J. W. Ruberti, *Rapid cryofixation/freeze fracture for the study of nanobubbles at solid-liquid interfaces*, App. Phys. Lett. **84**, 4759 (2004).

[26] X. H. Zhang, J. M. Ren, H. J. Yang, Y. H. He, J. F. Tan, and G. G. Qiao, *From Transient Nanodroplets to Permanent Nanolenses*, Soft Matter **8**, 4314 (2012).

[27] S. Schlücker, *Surface-Enhanced raman spectroscopy: Concepts and chemical applications*, Angew. Chemie Int. Ed. **53**, 4756 (2014).

[28] G. M. Whitesides, *The origins and the future of microfluidics*, Nature **442**, 368 (2006).

[29] T. Squires and S. Quake, *Microfluidics: Fluid physics at the nanoliter scale*, Rev. Mod. Phys. **77**, 977 (2005).

[30] P. Garstecki, M. J. Fuerstman, H. A. Stone, and G. M. Whitesides, *Formation of droplets and bubbles in a microfluidic T-junction: scaling and mechanism of break-up*, Lab on Chip **6**, 437 (2006).

[31] J. C. T. Eijkel and A. van den Berg, *Nanofluidics: what is it and what can we expect from it?*, Microfluidics and Nanofluidics **1**, 249 (2005).

[32] A. J. deMello, *Control and detection of chemical reactions in microfluidic systems*, Nature **442**, 394 (2006).

[33] S. Lach, S. M. Yoon, and B. A. Grzybowski, *Tactic, reactive, and functional droplets outside of equilibrium*, Chem. Soc. Rev. **45**, 4766 (2016).

[34] V. Spandan, D. Lohse, M. D. de Tullio, and R. Verzicco, *A fast moving least squares approximation with adaptive Lagrangian mesh refinement for large scale immersed boundary simulations*, J. Comp. Phys. **375**, 228 (2018).

[35] C. Diddens, *Detailed finite element method modeling of evaporating multi-component droplets*, J. Comp. Phys. **340**, 670 (2017).

[36] M. Heil and A. L. Hazel, *Fluid-structure interaction* (Springer, Berlin, 2006), pp. 19–49.

[37] M. Heil and A. L. Hazel, *Fluid-structure interaction in internal physiological flows*, Annu. Rev. Fluid Mech. **43**, 141 (2011).

[38] C. Diddens, H. Tan, P. Lv, M. Versluis, J. G. M. Kuerten, X. Zhang, and D. Lohse, *Evaporating pure, binary and ternary droplets: thermal effects and axial symmetry breaking*, J. Fluid Mech. **823**, 470 (2017).

[39] Y. Li, C. Diddens, A. Prosperetti, K. L. Chong, X. Zhang, and D. Lohse, *Bouncing Oil Droplet in a Stratified Liquid and its Sudden Death*, Phys. Rev. Lett. **122**, 154502 (2019).

[40] Y. Li, C. Diddens, P. Lv, H. Wijshoff, M. Versluis, and D. Lohse, *Gravitational effect in evaporating binary microdroplets*, Phys. Rev. Lett. **122**, 114501 (2019).

[41] J. H. Seo and R. Mittal, *A sharp-interface immersed boundary method with improved mass conservation and reduced spurious pressure oscillations*, J. Comp. Phys. **230**, 7347 (2011).

[42] L. Bao, V. Spandan, Y. Yang, B. Dyett, R. Verzicco, D. Lohse, and X. Zhang, *Flow-induced dissolution of femtoliter surface droplet arrays*, Lab on Chip **18**, 1066 (2018).

[43] X. Zhu, R. Verzicco, X. Zhang, and D. Lohse, *Diffusive interaction of multiple surface nanobubbles: shrinkage, growth, and coarsening*, Soft Matter **14**, 2006 (2018).

[44] J. Kim, *Phase-field models for multi-component fluid flows*, Commun. in Comput. Phys. **12**, 613 (2012).

[45] P. G. Moerman, P. C. Hohenberg, E. Vanden-Eijnden, and J. Brujic, *Emulsion patterns in the wake of a liquid–liquid phase separation front*, Proc. Nat. Acad. Sci. **115**, 3599 (2018).

[46] M. Sussman, P. Smereka, and S. Osher, *A level set approach for computing solutions to incompressible two-phase flow*, J. Comp. Phys. **114**, 146 (1994).

[47] J. A. Sethian and P. Smereka, *Level set methods for fluid interfaces*, Annu. Rev. Fluid Mech. **35**, 341 (2003).

[48] C. C. de Langavant, A. Guittet, M. Theillard, F. Temprano-Coleto, and F. Gibou, *Level-set simulations of soluble surfactant driven flows*, J. Comp. Phys. **348**, 271 (2017).

[49] F. Gibou, R. Fedkiw, and S. Osher, *A review of level-set methods and some recent applications*, J. Comp. Phys. **353**, 82 (2018).

[50] S. Chen and G. D. Doolen, *Lattice Boltzmann method for fluid flows*, Annu. Rev. Fluid Mech. **30**, 329 (1998).

[51] C. K. Aidun and J. R. Clausen, *Lattice-Boltzmann method for complex flows*, Annu. Rev. Fluid Mech. **42**, 439 (2010).

[52] P. Perlekar, R. Benzi, H. J. Clercx, D. R. Nelson, and F. Toschi, *Spinodal decomposition in homogeneous and isotropic turbulence*, Phys. Rev. Lett. **112**, 014502 (2014).

[53] D. Hessling, Q. Xie, and J. Harting, *Diffusion dominated evaporation in multicomponent lattice Boltzmann simulations*, The Journal of chemical physics **146**, 054111 (2017).

[54] J. Koplik and J. R. Banavar, *Continuum Deductions from Molecular Hydrodynamics*, Annu. Rev. Fluid Mech. **27**, 257 (1995).

[55] D. Frenkel and B. Smit, *Understanding molecular simulations: From algorithm to applications* (Academic Press, San Diego, 1996).

[56] E. Lauga, M. P. Brenner, and H. A. Stone, in *Handbook of Experimental Fluid Dynamics*, edited by C. Tropea, A. Yarin, and J. F. Foss (Springer, New York, 2007), pp. 1219–1240.

[57] L. Bocquet and E. Charlaix, *Nanofluidics, from bulk to interfaces*, Chem. Soc. Rev. **39**, 1073 (2010).

[58] S. Maheshwari, M. van der Hoef, X. Zhang, and D. Lohse, *Stability of Surface Nanobubbles: A Molecular Dynamics Study*, Langmuir **32**, 11116 (2016).

[59] S. Maheshwari, M. van der Hoef, J. Rodriguez Rodriguez, and D. Lohse, *Leakiness of Pinned Neighboring Surface Nanobubbles Induced by Strong Gas-Surface Interaction*, ACS Nano **12**, 2603 (2018).

[60] D. Lohse, *Bubble Puzzles: From fundamentals to applications*, Phys. Rev. Fluids **3**, 110504 (2018).

[61] N. Young, J. Goldstein, and M. J. Block, *The motion of bubbles in a vertical temperature gradient*, J. Fluid Mech. **6**, 350 (1959).

[62] C. Jin, C. Krüger, and C. C. Maass, *Chemotaxis and autochemotaxis of self-propelling droplet swimmers*, Proc. Nat. Acad. Sci. **114**, 5089 (2017).

[63] S. Michelin, E. Lauga, and D. Bartolo, *Spontaneous autophoretic motion of isotropic particles*, Phys/ Fluids **25**, 061701 (2013).

[64] C. Krüger, G. Klös, C. Bahr, and C. C. Maass, *Curling liquid crystal microswimmers: A cascade of spontaneous symmetry breaking*, Phys. Rev. Lett. **117**, 048003 (2016).

[65] W.-F. Hu, T.-S. Lin, S. Rafai, and C. Misbah, *Chaotic Swimming of Phoretic Particles*, Phys. Rev. Lett. **123**, 238004 (2019).

[66] J. L. Anderson, *Colloid transport by interfacial forces*, Ann. Rev. Fluid Mech. **21**, 61 (1989).

[67] J. L. Anderson, M. E. Lowell, and D. C. Prieve, *Motion of a particle generated by chemical gradients Part 1. Non-electrolytes*, J. Fluid Mech. **117**, 107 (1982).

[68] Z. Izri, M. N. Van Der Linden, S. Michelin, and O. Dauchot, *Self-propulsion of pure water droplets by spontaneous Marangoni-stress-driven motion*, Phys. Rev. Lett. **113**, 248302 (2014).

[69] S. Marbach, H. Yoshida, and L. Bocquet, *Osmotic and diffusio-osmotic flow generation at high solute concentration. I. Mechanical approaches*, J. Chem. Phys. **146**, 194701 (2017).

[70] D. C. Prieve, S. M. Malone, A. S. Khair, R. F. Stout, and M. Y. Kanj, *Diffusiophoresis of charged colloidal particles in the limit of very high salinity*, Proc. Nat. Acad. Sci. **116**, 18257 (2019).

[71] F. Yang, S. Shin, and H. A. Stone, *Diffusiophoresis of a charged drop*, J. Fluid Mech. **852**, 37 (2018).

[72] M. Morozov and S. Michelin, *Nonlinear dynamics of a chemically-active drop: From steady to chaotic self-propulsion*, J. Chem. Phys. **150**, 044110 (2019).

[73] S. Karpitschka and H. Riegler, *Quantitative experimental study on the transition between fast and delayed coalescence of sessile droplets with different but completely miscible liquids*, Langmuir **26**, 11823 (2010).

[74] S. Karpitschka and H. Riegler, *Noncoalescence of sessile drops from different but miscible liquids: hydrodynamic analysis of the twin drop contour as a self-stabilizing traveling wave*, Phys. Rev. Lett. **109**, 066103 (2012).

[75] R. B. Koldeweij, B. F. Van Capelleveen, D. Lohse, and C. W. Visser, *Marangoni-driven spreading of miscible liquids in the binary pendant drop geometry*, Soft matter **15**, 8525 (2019).

[76] C. W. Visser, T. Kamperman, L. P. Karbaat, D. Lohse, and M. Karperien, *In-air microfluidics enables rapid fabrication of emulsions, suspensions, and 3D modular (bio) materials*, Science Advances **4**, eaao1175 (2018).

[77] H. Yu, P. Kant, B. Dyett, D. Lohse, and X. Zhang, *Splitting droplet through coalescence of two different three-phase contact lines*, Soft Matter **15**, 6055 (2019).

[78] H. Riegler and P. Lazar, *Delayed coalescence behavior of droplets with completely miscible liquids*, Langmuir **24**, 6395 (2008).

[79] Y. Yeo, O. A. Basaran, and K. Park, *A new process for making reservoir-type microcapsules using ink-jet technology and interfacial phase separation*, J. Controlled Release **93**, 161 (2003).

[80] S. Berg, *Marangoni-driven spreading along liquid-liquid interfaces*, Phys. Fluids **21**, 032105 (2009).

[81] F. Wodlei, J. Sebilleau, J. Magnaudet, and V. Pimienta, *Marangoni-driven flower-like patterning of an evaporating drop spreading on a liquid substrate*, Nature Communications **9**, 820 (2018).

[82] M. Jehannin, S. Charton, S. Karpitschka, T. Zemb, H. Moehwald, and H. Riegler, *Periodic precipitation patterns during coalescence of reacting sessile droplets*, Langmuir **31**, 11484 (2015).

[83] W. Paxton, K. Kistler, C. Olmeda, A. Sen, S. St Angelo, Y. Cao, T. Mallouk, P. Lammert, and V. Crespi, *Catalytic nanomotors: Autonomous movement of striped nanorods*, J. Am. Chem. Soc. **126**, 13424 (2004).

[84] R. Golestanian, T. B. Liverpool, and A. Ajdari, *Propulsion of a molecular machine by asymmetric distribution of reaction products*, Phys. Rev. Lett. **94**, 220801 (2005).

[85] H.-R. Jiang, N. Yoshinaga, and M. Sano, *Active motion of a Janus particle by self-thermophoresis in a defocused laser beam*, Phys. Rev. Lett. **105**, 268302 (2010).

[86] I. Buttinoni, J. Bialké, F. Kümmel, H. Löwen, C. Bechinger, and T. Speck, *Dynamical clustering and phase separation in suspensions of self-propelled colloidal particles*, Phys. Rev. Lett. **110**, 238301 (2013).

[87] S. Michelin and E. Lauga, *Phoretic self-propulsion at finite Péclet numbers*, J. Fluid Mech. **747**, 572 (2014).

[88] A. Golovin, Y. P. Gupalo, and Y. S. Ryazantsev, *Change in shape of drop moving due to the chemithermocapillary effect*, J. Appl. Mech. and Tech. Phys. **30**, 602 (1989).

[89] A. Y. Rednikov, Y. S. Ryazantsev, and M. G. Velarde, *Drop motion with surfactant transfer in a homogeneous surrounding*, Phys. Fluids **6**, 451 (1994).

[90] M. Schmitt and H. Stark, *Swimming active droplet: A theoretical analysis*, EPL **101**, 44008 (2013).

[91] M. Morozov and S. Michelin, *Self-propulsion near the onset of Marangoni instability of deformable active droplets*, J. Fluid Mech. **860**, 711 (2019).

[92] B. Abécassis, C. Cottin-Bizonne, C. Ybert, A. Ajdari, and L. Bocquet, *Boosting migration of large particles by solute contrasts*, Nature Materials **7**, 785 (2008).

[93] J. Palacci, B. Abecassis, C. Cottin-Bizonne, C. Ybert, and L. Bocquet, *Colloidal Motility and Pattern Formation under Rectified Diffusiophoresis*, Phys. Rev. Lett. **104**, 138302 (2010).

[94] A. Banerjee, I. Williams, R. N. Azevedo, M. E. Helgeson, and T. M. Squires, *Soluto-inertial phenomena: Designing long-range, long-lasting, surface-specific interactions in suspensions*, Proc. Nat. Acad. Sci. **113**, 8612 (2016).

[95] A. Banerjee and T. M. Squires, *Long-range, selective, on-demand suspension interactions: Combining and triggering soluto-inertial beacons*, Science Advances **5**, eaax1893 (2019).

[96] M. Suga, S. Suda, M. Ichikawa, and Y. Kimura, *Self-propelled motion switching in nematic liquid crystal droplets in aqueous surfactant solutions*, Physical Review E **97**, 062703 (2018).

[97] S. Thutupalli, R. Seemann, and S. Herminghaus, *Swarming behavior of simple model squirmers*, New J. Phys. **13**, 073021 (2011).

[98] J. Palacci, S. Sacanna, A. P. Steinberg, D. J. Pine, and P. M. Chaikin, *Living crystals of light-activated colloidal surfers*, Science **339**, 936 (2013).

[99] P. G. Moerman, H. W. Moyses, E. B. Van Der Wee, D. G. Grier, A. Van Blaaderen, W. K. Kegel, J. Groenewold, and J. Brujic, *Solute-mediated interactions between active droplets*, Phys. Rev. E **96**, 032607 (2017).

[100] K. Lippera, M. Morozov, M. Benzaquen, and S. Michelin, *Collisions and rebounds of chemically-active droplets*, J. Fluid Mech. **886**, A17 (2020).

[101] A. A. Peña and C. A. Miller, *Solubilization rates of oils in surfactant solutions and their relationship to mass transport in emulsions*, Adv. Colloid and Interface Sci. **123**, 241 (2006).

[102] S. Herminghaus, C. C. Maass, C. Krüger, S. Thutupalli, L. Goehring, and C. Bahr, *Interfacial mechanisms in active emulsions*, Soft Matter **10**, 7008 (2014).

[103] B. V. Hokmabad, K. A. Baldwin, C. Krüger, C. Bahr, and C. C. Maass, *Topological stabilization and dynamics of self-propelling nematic shells*, Phys. Rev. Lett. **123**, 178003 (2019).

[104] P. Poesio, G. P. Beretta, and T. Thorsen, *Dissolution of a liquid microdroplet in a non-ideal liquid-liquid mixture far from thermodynamic equilibrium*, Phys. rev. Lett. **103**, 064501 (2009).

[105] I. Lagzi, S. Soh, P. J. Wesson, K. P. Browne, and B. A. Grzybowski, *Maze solving by chemotactic droplets*, J. Am. Chem. Soc. **132**, 1198 (2010).

[106] J. Cejkova, M. Novak, F. Stepanek, and M. M. Hanczyc, *Dynamics of chemotactic droplets in salt concentration gradients*, Langmuir **30**, 11937 (2014).

[107] P. S. Epstein and M. S. Plesset, *On the stability of gas bubbles in liquid-gas solutions*, J. Chem. Phys. **18**, 1505 (1950).

[108] P. B. Duncan and D. Needham, *Microdroplet dissolution into a second-phase solvent using a micropipet technique: test of the Epstein-Plesset model for an aniline-water system*, Langmuir **22**, 4190 (2006).

[109] R. G. Picknett and R. Bexon, *The evaporation of sessile or pendant drops in still air*, J. Colloid Interface Sci. **61**, 336 (1977).

[110] R. D. Deegan, O. Bakajin, T. F. Dupont, G. Huber, S. R. Nagel, and T. A. Witten, *Capillary flow as the cause of ring stains from dried liquid drops*, Nature **389**, 827 (1997).

[111] H. Hu and R. G. Larson, *Evaporation of a Sessile Droplet on a Substrate*, J. Phys. Chem. B **106**, 1334 (2002).

[112] Y. O. Popov, *Evaporative deposition patterns: Spatial dimensions of the deposit*, Phys. Rev. E **71**, 036313 (2005).

[113] H. Gelderblom, A. G. Marin, H. Nair, A. van Houselt, L. Lefferts, J. H. Snoeijer, and D. Lohse, *How water droplets evaporate on a superhydrophobic substrate*, Phys. Rev. E **83**, 026306 (2011).

[114] J. M. Stauber, S. K. Wilson, B. R. Duffy, and K. Sefiane, *On the lifetimes of evaporating droplets*, J. Fluid Mech. **744**, R2 (2014).

[115] E. Dietrich, S. Wildeman, C. W. Visser, K. Hofhuis, E. S. Kooij, H. J. W. Zandvliet, and D. Lohse, *Role of natural convection in the dissolution of sessile droplets*, J. Fluid Mech. **794**, 45 (2016).

[116] G. Laghezza, E. Dietrich, J. M. Yeomans, R. Ledesma-Aguilar, E. S. Kooij, H. J. W. Zandvliet, and D. Lohse, *Collective and convective effects compete in patterns of dissolving surface droplets*, Soft Matter **12**, 5787 (2016).

[117] O. Carrier, N. Shahidzadeh-Bonn, R. Zargar, M. Aytouna, M. Habibi, J. Eggers, and D. Bonn, *Evaporation of water: evaporation rate and collective effects*, J. Fluid Mech. **798**, 774 (2016).

[118] S. Michelin, E. Guérin, and E. Lauga, *Collective dissolution of microbubbles*, Phys. Rev. Fluids **3**, 043601 (2018).

[119] A. W. Wray, B. R. Duffy, and S. K. Wilson, *Competitive evaporation of multiple sessile droplets*, J. Fluid Mech. **884**, A45 (2020).

[120] K. L. Chong, Y. Li, C. S. Ng, R. Verzicco, and D. Lohse, *Convection-dominated dissolution for single and multiple immersed sessile droplets*, J. Fluid Mech. **892**, A21 (2020).

[121] R. D. Deegan, O. Bakajin, T. F. Dupont, G. Huber, S. R. Nagel, and T. A. Witten, *Contact line deposits in an evaporating drop*, Phys. Rev. E **62**, 756 (1998).

[122] L. Scriven and C. Sternling, *The Marangoni effects*, Nature **187**, 186 (1960).

[123] H. Hu and R. G. Larson, *Analysis of the effects of Marangoni stresses on the microflow in an evaporating sessile droplet*, Langmuir **21**, 3972 (2005).

[124] R. Bennacer and K. Sefiane, *Vortices, dissipation and flow transition in volatile binary drops*, J. Fluid Mech. **749**, 649 (2014).

[125] H. Kim, F. Boulogne, E. Um, I. Jacobi, E. Button, and H. A. Stone, *Controlled Uniform Coating from the Interplay of Marangoni Flows and Surface-Adsorbed Macromolecules*, Phys. Rev. Lett. **116**, 124501 (2016).

[126] E. Dietrich, M. Rump, P. Lv, E. S. Kooij, H. J. W. Zandvliet, and D. Lohse, *Segregation in dissolving binary component sessile droplets*, J. Fluid Mech. **812**, 349 (2017).

[127] S. Karpitschka, F. Liebig, and H. Riegler, *Marangoni contraction of evaporating sessile droplets of binary mixtures*, Langmuir **33**, 4682 (2017).

[128] H. Kim, K. Muller, O. Shardt, S. Afkhami, and H. A. Stone, *Solutal Marangoni flows of miscible liquids drive transport without surface contamination*, Nature Physics **13**, 1105 (2017).

[129] Y. Li, P. Lv, C. Diddens, H. Tan, H. Wijshoff, M. Versluis, and D. Lohse, *Evaporation-triggered segregation of sessile binary droplets*, Phys. Rev. Lett. **120**, 224501 (2018).

[130] H. Kim and H. A. Stone, *Direct measurement of selective evaporation of binary mixture droplets by dissolving materials*, J. Fluid Mech. **850**, 769 (2018).

[131] A. Edwards, P. Atkinson, C. Cheung, H. Liang, D. Fairhurst, and F. Ouali, *Density-driven flows in evaporating binary liquid droplets*, Phys. Rev. Lett. **121**, 184501 (2018).

[132] A. Marin, S. Karpitschka, D. Noguera-Marín, M. A. Cabrerizo-Vílchez, M. Rossi, C. J. Kähler, and M. A. R. Valverde, *Solutal Marangoni flow as the cause of ring stains from drying salty colloidal drops*, Phys. Rev. Fluids **4**, 041601 (2019).

[133] A. E. Hosoi and J. W. M. Bush, *Evaporative instabilities in climbing films*, J. Fluid Mech. **442**, 217 (2001).

[134] S. Shin, I. Jacobi, and H. A. Stone, *Bénard-Marangoni instability driven by moisture absorption*, EPL **113**, 24002 (2016).

[135] S. Karpitschka, *The value of a fading tracer*, J. Fluid Mech. **856**, 1 (2018).

[136] C. Diddens, Y. Li, and D. Lohse, *Competing Marangoni and Rayleigh convection in evaporating binary droplets*, J. Fluid Mech. **xx**, xxx (2020).

[137] Y. Li, C. Diddens, T. Segers, H. Wijshoff, M. Verluis, and D. Lohse, *Rayleigh-Taylor instability by segregation in an evaporating multicomponent microdroplet*, J. Fluid Mech. **xxx**, xxx (2020).

[138] L. Keiser, H. Bense, P. Colinet, J. Bico, and E. Reyssat, *Marangoni bursting: evaporation-induced emulsification of binary mixtures on a liquid layer*, Phys. Rev. Lett. **118**, 074504 (2017).

[139] G. Durey, H. Kwon, Q. Magdelaine, M. Casiulis, J. Mazet, L. Keiser, H. Bense, P. Colinet, J. Bico, and E. Reyssat, *Marangoni bursting: Evaporation-induced emulsification of a two-component droplet*, Phys. Rev. Fluids **3**, 100501 (2018).

[140] J. F. Hernández-Sánchez, A. Eddi, and J. H. Snoeijer, *Marangoni spreading due to a localized alcohol supply on a thin water film*, Phys. Fluids **27**, 032003 (2015).

[141] D. Dedovets, C. Monteux, and S. Deville, *Five-dimensional imaging of freezing emulsions with solute effects*, Science **360**, 303 (2018).

[142] F. Pregl, *Die quantitative organische Mikroanalyse* (Springer, Berlin, 1917).

[143] M. Rezaee, Y. Assadi, M. R. M. Hosseinia, E. Aghaee, F. Ahmadi, and S. Berijani, *Determination of organic compounds in water using dispersive liquid-liquid microextraction*, J. Chromatography A **1116**, 1 (2006).

[144] S. Maheshwari, M. Van Der Hoef, A. Prosperetti, and D. Lohse, *Molecular dynamics study of multicomponent droplet dissolution in a sparingly miscible liquid*, J. Fluid Mech. **833**, 54 (2017).

[145] S. Chu and A. Prosperetti, *Dissolution and growth of a multicomponent drop in an immiscible liquid*, J. Fluid Mech. **798**, 787 (2016).

[146] D. Lohse, *Towards controlled liquid-liquid microextraction*, J. Fluid Mech. **804**, 1 (2016).

[147] S. Deville, *Freezing colloids: observations, principles, control, and use: applications in materials science, life science, earth science, food science, and engineering* (Springer, Berlin, 2017).

[148] S. Vitale and J. Katz, *Liquid droplet dispersions formed by homogeneous liquid-liquid nucleation: "The ouzo effect"*, Langmuir **19**, 4105 (2003).

[149] F. Ganachaud and J. Katz, *Nanoparticles and nanocapsules created using the Ouzo effect: spontaneous emulsification as an alternative to ultrasonic and high-shear devices*, Chem. Phys. Chem **6**, 209 (2005).

[150] E. Lepeltier, C. Bourgaux, and P. Couvreur, *Nanoprecipitation and the "Ouzo effect": Application to drug delivery devices*, Adv. Drug Delivery Rev. **71**, 86 (2014).

[151] P. W. Voorhees, *The theory of Ostwald ripening*, J. Stat. Phys. **38**, 231 (1985).

[152] C. Solans, P. Izquierdo, J. Nolla, N. Azemar, and M. J. Garcia-Celma, *Nano-emulsions*, Current Opinion Colloid & Interface Sci. **10**, 102 (2005).

[153] T. N. Zemb, M. Klossek, T. Lopian, J. Marcus, S. Schöettl, D. Horinek, S. F. Prevost, D. Touraud, O. Diat, S. Mar***v***celja, *et al.*, *How to explain microemulsions formed by solvent mixtures without conventional surfactants*, Proc. Nat. Acad. Sci. **113**, 4260 (2016).

[154] J. Joanny and P. de Gennes, *A model for contact angle hysteresis*, J. Chem. Phys. **81**, 552 (1984).

[155] P. G. de Gennes, *Wetting: statics and dynamics*, Rev. Mod. Phys. **57**, 827 (1985).

[156] Y. Liu and X. Zhang, *Evaporation dynamics of nanodroplets and their anomalous stability on rough substrates*, Phys. Rev. E **88**, 012404 (2013).

[157] D. Lohse and X. Zhang, *Pinning and gas oversaturation imply stable single surface nanobubble*, Phys. Rev. E **91**, 031003(R) (2015).

[158] C. Solans, D. Morales, and M. Homs, *Spontaneous emulsification*, Current Opinion Colloid & Interface Sci. **22**, 88 (2016).

[159] T. Lopian, S. Schöttl, S. Prevost, S. Pellet-Rostaing, D. Horinek, W. Kunz, and T. Zemb, *Morphologies Observed in Ultraflexible Microemulsions with and without the Presence of a Strong Acid*, ACS Central Science **2**, 467 (2016).

[160] G. Taylor, *Dispersion of soluble matter in solvent flowing slowly through a tube*, Proc. Roy. Soc. London A **219**, 186 (1953).

[161] R. Aris, *On the dispersion of a solute in a fluid flowing through a tube*, Proc. Roy. Soc. London A **235**, 67 (1956).

[162] R. Aris, *On the dispersion of a solute by diffusion, convection and exchange between phases*, Proc. Roy. Soc. London A **252**, 538 (1959).

[163] H. Yu, S. Maheshwari, J. Zhu, D. Lohse, and X. Zhang, *Formation of surface nanodroplets facing a structured microchannel wall*, Lab on Chip **17**, 1496 (2017).

[164] X. Zhang, Z. Lu, H. Tan, L. Bao, Y. He, C. Sun, and D. Lohse, *Formation of surface nanodroplets under controlled flow conditions*, Proc. Nat. Acad. Sci. **112**, 9253 (2015).

[165] S. L. Anna, N. Bontoux, and H. A. Stone, *Formation of dispersions using flow focusing in microchannels*, Appl. Phys. Lett. **82**, 364 (2003).

[166] A. Utada, E. Lorenceau, D. Link, P. Kaplan, H. A. Stone, and D. Weitz, *Monodisperse double emulsions generated from a microcapillary device*, Science **308**, 537 (2005).

[167] M. F. Haase and J. Brujic, *Tailoring of High-Order Multiple Emulsions by the Liquid–Liquid Phase Separation of Ternary Mixtures*, Angew. Chemie Int. Ed/ **53**, 11793 (2014).

[168] H. Yu, Z. Lu, D. Lohse, and X. Zhang, *Gravitational Effect on the Formation of Surface Nanodroplets*, Langmuir **31**, 12628 (2015).

[169] B. Zeng, Y. Wang, X. Zhang, and D. Lohse, *Solvent Exchange in a Hele–Shaw Cell: Universality of Surface Nanodroplet Nucleation*, J. Phys. Chem. C **123**, 5571 (2019).

[170] L. Bao, Z. Werbiuk, D. Lohse, and Z. Zhang, *Controlling the growth modes of femtoliter sessile droplets nucleating on chemically patterned surfaces*, J. Phys. Chem. Lett. **7**, 1055 (2016).

[171] S. Peng, T. L. Mega, and X. Zhang, *Collective Effects in Microbubble Growth by Solvent Exchange*, Langmuir **32**, 11265 (2016).

[172] B. Dyett, A. Kiyama, M. Rump, Y. Tagawa, D. Lohse, and X. Zhang, *Growth dynamics of surface nanodroplets during solvent exchange at varying flow rates*, Soft Matter **14**, 5197 (2018).

[173] S. Peng, D. Lohse, and X. Zhang, *Spontaneous Pattern Formation of Surface Nanodroplets from Competitive Growth*, ACS Nano **9**, 11916 (2015).

[174] C. Xu, H. Yu, S. Peng, Z. Lu, L. Lei, D. Lohse, and X. Zhang, *Collective interactions in the nucleation and growth of surface droplets*, Soft Matter **13**, 937 (2017).

[175] B. Dyett, H. Hao, D. Lohse, and X. Zhang, *Coalescence driven self-organization of growing nanodroplets around a microcap*, Soft Matter **14**, 2628 (2018).

[176] H. Schlichting, *Boundary layer theory*, 7th ed. (McGraw Hill, New York, 1979).

[177] X. Zhang, J. Wang, L. Bao, E. Dietrich, R. C. A. van der Veen, S. Peng, J. Friend, H. J. W. Zandvliet, L. Yeo, and D. Lohse, *Mixed mode of dissolving immersed microdroplets at a solid-water interface*, Soft Matter **11**, 1889 (2015).

[178] H. Tan, C. Diddens, M. Versluis, H.-J. Butt, D. Lohse, and X. Zhang, *Self-wrapping of an ouzo drop induced by evaporation on a superamphiphobic surface*, Soft Matter **13**, 2749 (2017).

[179] H. Tan, C. Diddens, A. A. Mohammed, J. Li, M. Versluis, X. Zhang, and D. Lohse, *Micro-droplet nucleation by dissolution of a multicomponent drop in a host liquid*, J. Fluid Mech. **870**, 217 (2019).

[180] J. S. Kirkaldy and L. Brown, *Diffusion behaviour in ternary, multiphase systems*, Canadian Metallurgical Quarterly **2**, 89 (1963).

[181] K. J. Ruschak and C. A. Miller, *Spontaneous emulsification in ternary systems with mass transfer*, Industrial & Engineering Chemistry Fundamentals **11**, 534 (1972).

[182] C. A. Miller and P. Neogi, *Interfacial phenomena: equilibrium and dynamic effects* (CRC Press, Boca Raton, 2007), Vol. 139.

[183] J. Otero, S. Meeker, and P. S. Clegg, *Compositional ripening of particle-stabilized drops in a three-liquid system*, Soft Matter **14**, 3783 (2018).

[184] C.-H. Choi, D. A. Weitz, and C.-S. Lee, *One step formation of controllable complex emulsions: from functional particles to simultaneous encapsulation of hydrophilic and hydrophobic agents into desired position*, Adv. Materials **25**, 2536 (2013).

[185] L. D. Zarzar, V. Sresht, E. M. Sletten, J. A. Kalow, D. Blankschtein, and T. M. Swager, *Dynamically reconfigurable complex emulsions via tunable interfacial tensions*, Nature **518**, 520 (2015).

[186] Z. Lu, M. H. K. Schaarsberg, X. Zhu, L. Y. Yeo, D. Lohse, and X. Zhang, *Universal nanodroplet branches from confining the Ouzo effect*, Proc. Nat. Acad. Sci **114**, 10332 (2017).

[187] R. Hajian and S. Hardt, *Formation and lateral migration of nanodroplets via solvent shifting in a microfluidic device*, Microfluidics and Nanofluidics **19**, 1281 (2015).

[188] M. Rezaee, Y. Yamini, and M. Faraji, *Evolution of dispersive liquid-liquid microextraction method*, J. Chromatography A **1217**, 2342 (2010).

[189] A. Zgola-Grzeskowiak and T. Grzeskowiak, *Dispersive liquid-liquid microextraction*, Trends in Analytical Chem. **30**, 1382 (2011).

[190] J. M. P. Guiterrez, T. Hinkley, J. W. Taylor, K. Yanev, and L. Cronin, *Evolution of oil droplets in a chemorobotic platform*, Nature Comm. **5**, 5571 (2014).

[191] J. A. Ocaña-González, R. Fernández-Torres, M. Á. Bello-López, and M. Ramos-Payán, *New developments in microextraction techniques in bioanalysis. A review*, Analytica Chimica Acta **905**, 8 (2016).

[192] M. Li, B. Dyett, H. Yu, V. Bansal, and X. Zhang, *Functional Femtoliter Droplets for Ultrafast Nanoextraction and Supersensitive Online Microanalysis*, Small **15**, 1804683 (2019).

[193] M. Li, B. Dyett, and X. Zhang, *Automated Femtoliter Droplet-Based Determination of Oil–Water Partition Coefficient*, Analytical Chemistry **91**, 10371 (2019).

[194] J. Qian, D. Yamada, Z. Wei, R. Yukisada, Y. Tagawa, J. M. Shaw, and X. Zhang, *One-Step Nanoextraction and Ultrafast Microanalysis Based on Nanodroplet Formation in an Evaporating Ternary Liquid Microfilm*, Advanced Materials Technologies **5**, 1900740 (2020).

[195] J. Gutiérrez, C. González, A. Maestro, I. Solé, C. Pey, and J. Nolla, *Nano-emulsions: New applications and optimization of their preparation*, Cur. Opinion in Colloid & Interface Sci. **13**, 245 (2008).

[196] C. Zhang, V. J. Pansare, R. K. Prud'homme, and R. D. Priestley, *Flash nanoprecipitation of polystyrene nanoparticles*, Soft Matter **8**, 86 (2012).

[197] M. Akbulut, P. Ginart, M. E. Gindy, C. Theriault, K. H. Chin, W. Soboyejo, and R. K. Prud'homme, *Generic Method of Preparing Multifunctional Fluorescent Nanoparticles Using Flash NanoPrecipitation*, Adv. Funct. Mater. **19**, 718 (2009).

[198] Z. Zeng, C. Dong, P. Zhao, Z. Liu, L. Liu, H.-Q. Mao, K. W. Leong, X. Gao, and Y. Chen, *Scalable Production of Therapeutic Protein Nanoparticles Using Flash Nanoprecipitation*, Adv. Healthc. Mater. **8**, 1801010 (2019).

[199] G. Coquerel, *Crystallization of molecular systems from solution: phase diagrams, supersaturation and other basic concepts*, Chem. Soc. Rev. **43**, 2286 (2014).

[200] X. Sun, Y. Zhang, G. Chen, and Z. Gai, *Application of nanoparticles in enhanced oil recovery: a critical review of recent progress*, Energies **10**, 345 (2017).

[201] F. Rao and Q. Liu, *Froth treatment in Athabasca oil sands bitumen recovery process: A review*, Energy Fuels **27**, 7199 (2013).

[202] L. He, F. Lin, X. Li, H. Sui, and Z. Xu, *Interfacial sciences in unconventional petroleum production: from fundamentals to applications*, Chem. Soc. Rev. **44**, 5446 (2015).

[203] S. Crossley, J. Faria, M. Shen, and D. E. Resasco, *Solid Nanoparticles that Catalyze Biofuel Upgrade Reactions at the Water/Oil Interface*, Science **327**, 68 (2010).

[204] T. Z. Jia, K. Chandru, Y. Hongo, R. Afrin, T. Usui, K. Myojo, and H. J. Cleaves, *Membraneless polyester microdroplets as primordial compartments at the origins of life*, Proc. Nat. Acad. Sci. **116**, 15830 (2019).

[205] D. Zwicker, M. Decker, S. Jaensch, A. A. Hyman, and F. Jülicher, *Centrosomes are autocatalytic droplets of pericentriolar material organized by centrioles*, Proc. Nat. Acad. Sci. **111**, 2636 (2014).

[206] D. Zwicker, R. Seyboldt, C. A. Weber, A. A. Hyman, and F. Jülicher, *Growth and division of active droplets provides a model for protocells*, Nature Physics **13**, 408 (2017).

[207] R. Golestanian, *Division for multiplication*, Nature Physics **13**, 323 (2017).

[208] J. K. Lee, S. Kim, H. G. Nam, and R. N. Zare, *Microdroplet fusion mass spectrometry for fast reaction kinetics*, Proc. Nat. Acad. Sci. **112**, 3898 (2015).

[209] J. K. Lee, D. Samanta, H. G. Nam, and R. N. Zare, *Micrometer-Sized Water Droplets Induce Spontaneous Reduction*, J. Am. Chem. Soc. **141**, 10585 (2019).

[210] A. Fallah-Araghi, K. Meguellati, J.-C. Baret, A. El Harrak, T. Mangeat, M. Karplus, S. Ladame, C. M. Marques, and A. D. Griffiths, *Enhanced chemical synthesis at soft interfaces: A universal reaction-adsorption mechanism in microcompartments*, Phys. Rev. Lett. **112**, 028301 (2014).

[211] J. T. G. Overbeek and M. J. Voorn, *Phase separation in polyelectrolyte solutions. Theory of complex coacervation*, J. Cell. Comp. Physiol. **49**, 7 (1957).

[212] E. Kizilay, A. Kayitmazer, and P. Dubin, *Complexation and coacervation of polyelectrolytes with oppositely charged colloids*, Adv. Colloid Interface Sci. **167**, 24 (2011).

[213] A. I. Oparin *et al.*, *The Origin of Life on the Earth.* (Oliver & Boyd, Edinburgh & London, 1957).

[214] Y. Shin and C. P. Brangwynne, *Liquid phase condensation in cell physiology and disease*, Science **357**, eaaf4382 (2017).

[215] S. Seo, S. Das, P. J. Zalicki, R. Mirshafian, C. D. Eisenbach, J. N. Israelachvili, J. H. Waite, and B. K. Ahn, *Microphase Behavior and Enhanced Wet-Cohesion of Synthetic Copolyampholytes Inspired by a Mussel Foot Protein*, J. Am. Chem. Soc. **137**, 9214 (2015).

[216] L.-W. Chang, T. K. Lytle, M. Radhakrishna, J. J. Madinya, J. Vélez, C. E. Sing, and S. L. Perry, *Sequence and entropy-based control of complex coacervates*, Nature Communications **8**, 1273 (2017).

[217] H. Wijshoff, *The dynamics of the piezo inkjet printhead operation*, Phys. Reports **491**, 77 (2010).

[218] M. Kuang, L. Wang, and Y. Song, *Controllable printing droplets for high-resolution patterns*, Adv. Materials **26**, 6950 (2014).

[219] S. D. Hoath, *Fundamentals of inkjet printing: the science of inkjet and droplets* (John Wiley & Sons, Weinheim, 2016).

[220] J. F. Dijksman, *Design of Piezo Inkjet Print Heads: From Acoustics to Applications* (Wiley-VCH, Weinheim, 2019).

[221] J. de Jong, H. Reinten, H. Wijshoff, M. van den Berg, K. Delescen, R. van Dongen, F. Mugele, M. Versluis, and D. Lohse, *Marangoni flow on an inkjet nozzle plate*, Appl. Phys. Lett. **91**, 204102 (2007).

[222] B. Beulen, J. de Jong, H. Reinten, M. van den Berg, H. Wijshoff, and R. van Dongen, *Flows on the nozzle plate of an inkjet printhead.*, Exp. Fluids **42**, 217 (2007).

[223] J. de Jong, R. Jeurissen, H. Borel, M. van den Berg, H. Wijshoff, H. Reinten, M. Versluis, A. Prosperetti, and D. Lohse, *Entrapped air bubbles in piezo-driven inkjet printing: Their effect on the droplet velocity*, Phys. Fluids **18**, 121511 (2006).

[224] A. Fraters, M. van den Berg, Y. de Loore, H. Reinten, H. Wijshoff, D. Lohse, M. Versluis, and T. Segers, *Inkjet Nozzle Failure by Heterogeneous Nucleation: Bubble Entrainment, Cavitation, and Diffusive Growth*, Phys. Rev. Applied **12**, 064019 (2019).

[225] W. Han and Z. Lin, *Learning from Coffee Rings: Ordered Structures Enabled by Controlled Evaporative Self-Assembly*, Angew. Chemie Int. Ed. **51**, 1534 (2012).

[226] Y. Cai and B.-m. Zhang-Newby, *Marangoni flow-induced self-assembly of hexagonal and stripelike nanoparticle patterns*, J. Am. Chem. Soc. **130**, 6076 (2008).

[227] E. Reverchon, I. De Marco, and E. Torino, *Nanoparticles production by supercritical antisolvent precipitation: a general interpretation*, J. Supercritical Fluids **43**, 126 (2007).

[228] H.-K. Chan and P. C. L. Kwok, *Production methods for nanodrug particles using the bottom-up approach*, Adv. Drug Delivery Reviews **63**, 406 (2011).

[229] W. Huang and C. Zhang, *Tuning the Size of Poly (lactic-co-glycolic Acid)(PLGA) Nanoparticles Fabricated by Nanoprecipitation*, Biotech. J. **13**, 1700203 (2018).

[230] L.-f. Zhang, *Indirect methods of detecting and evaluating inclusions in steel: a review*, J. Iron & Steel Res. Int. **13**, 1 (2006).

[231] A. Leenaars, J. Huethorst, and J. Van Oekel, *Marangoni drying: a new extremely clean drying process*, Langmuir **6**, 1701 (1990).

[232] J. Marra and J. Huethorst, *Physical principles of Marangoni drying*, Langmuir **7**, 2748 (1991).

[233] S. O'Brien, *On Marangoni drying: nonlinear kinematic waves in a thin film*, J. Fluid Mech. **254**, 649 (1993).

[234] A. Thess and W. Boos, *A model for Marangoni drying*, Phys. Fluids **11**, 3852 (1999).

[235] O. Matar and R. Craster, *Models for Marangoni drying*, Phys. Fluids **13**, 1869 (2001).

[236] H. F. Okorn-Schmidt, F. Holsteyns, A. Lippert, D. Mui, M. Kawaguchi, C. Lechner, P. E. Frommhold, T. Nowak, F. Reuter, M. B. Piqué, *et al.*, *Particle cleaning technologies to meet advanced semiconductor device process requirements*, ECS J. Solid State Sci. Tech. **3**, N3069 (2014).

[237] J. Bico, B. Roman, L. Moulin, and A. Boudaoud, *Adhesion: elastocapillary coalescence in wet hair*, Nature **432**, 690 (2004).

[238] C. Duprat, S. Protiere, A. Beebe, and H. A. Stone, *Wetting of flexible fibre arrays*, Nature **482**, 510 (2012).

[239] J. Bico, É. Reyssat, and B. Roman, *Elastocapillarity: When surface tension deforms elastic solids*, Annu. Rev. Fluid Mech. **50**, 629 (2018).

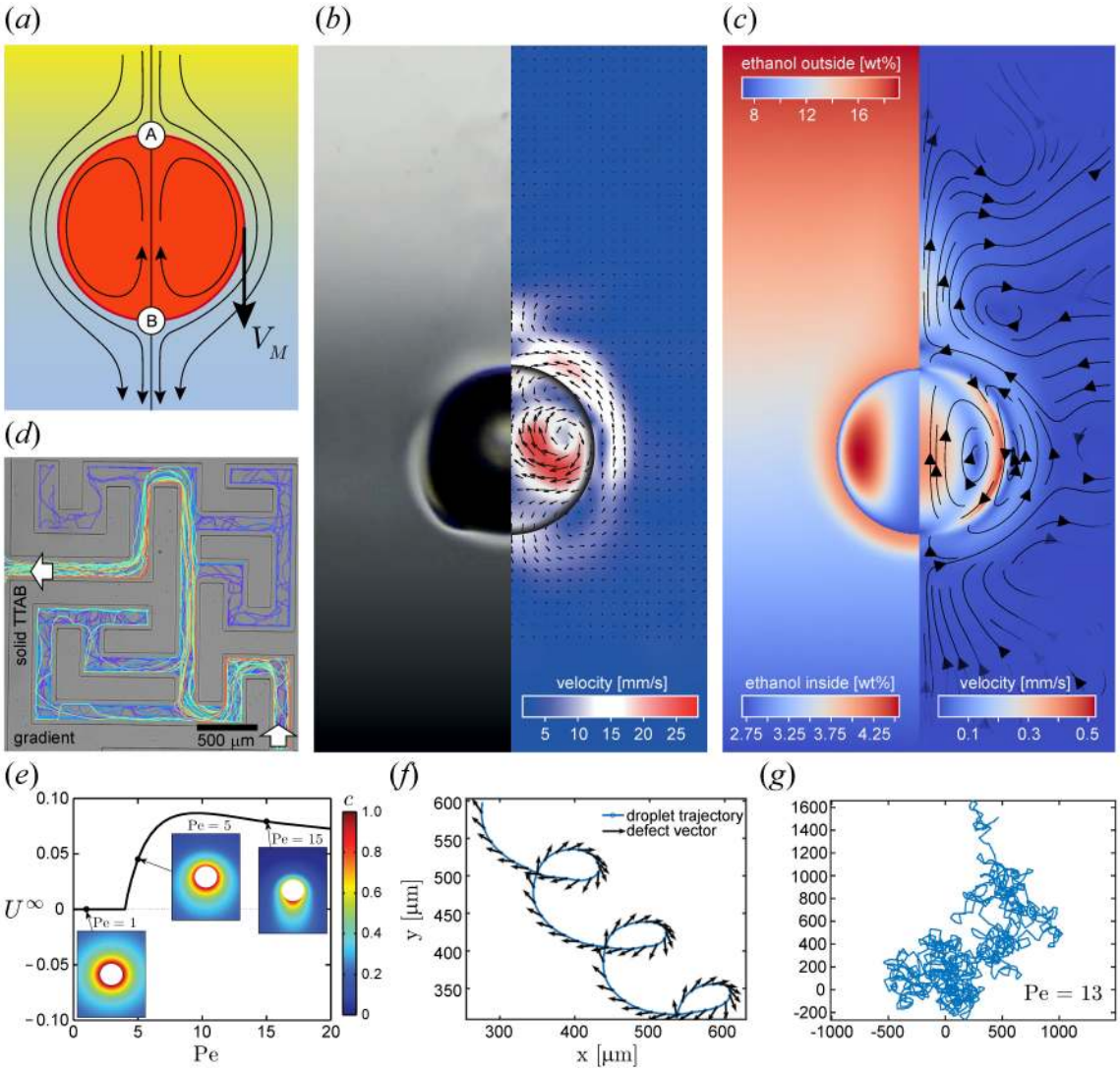

Figure 1: *(a) Immiscible droplet (red) in a concentration gradient, shown through the color gradient, with the heavier water in the bottom (bluish) and the lighter ethanol at the top (yellowish). We will stick to this color code in the sketches throughout the article. The surface tension at the top of the drop (A) is smaller than at the bottom (B), leading to some Marangoni flow, whose streamlines (calculated in the viscous limit, assuming constant density [61]) are shown (in the frame of reference of the drop). Also shown is the Marangoni velocity V_M. The velocity fields for a more complicated configuration of a partially (but poorly) miscible anise oil drop in an ethanol-water concentration gradient are shown in (b) (experimental, from a snapshot and from PIV images) and (c) (numerical result). On the right of each of these figures, the velocity field is shown, both as color code and as stream lines (in the lab frame). On the left, in (b) the snapshot is shown and in (c) the ethanol concentration inside and outside the anise oil drop (also shown in the lab frame). Figures (b) and (c) refer to the situation of ref. [39]. (d) Maze solving by chemotactic droplet swimmers: A chemical gradient of the ionic surfactant tetradecyltrimethylammonium bromide (TTAB) was imposed; the oil droplet propelling in the gradient inside the maze consists of the nematic liquid crystal 4-pentyl-4'-cyano-biphenyl. The trajectories of the swimmers that passed both entrance and exit points are shown, with the line color corresponding to the time in the experiment. Figure taken from ref. [62]. (e) Long-time spontaneous swimming velocity U^∞ as function of the Peclet number Pe. The concentration field around the droplet (or particle) is shown for three different Peclet numbers. A clear bifurcation towards droplet motion thanks to spontaneous symmetry breaking is seen at $Pe = 4$. Figure adapted from ref. [63]. (f) Curling nematic droplet ($R \approx 25\mu m$, phoretic) from the experiments of ref. [64], where the Peclet number is estimated to be larger than 4. (g) Chaotic droplet motion for a phoretic droplet with an even larger Peclet number $Pe = 13$. Figure taken from the numerical simulations of [65].*

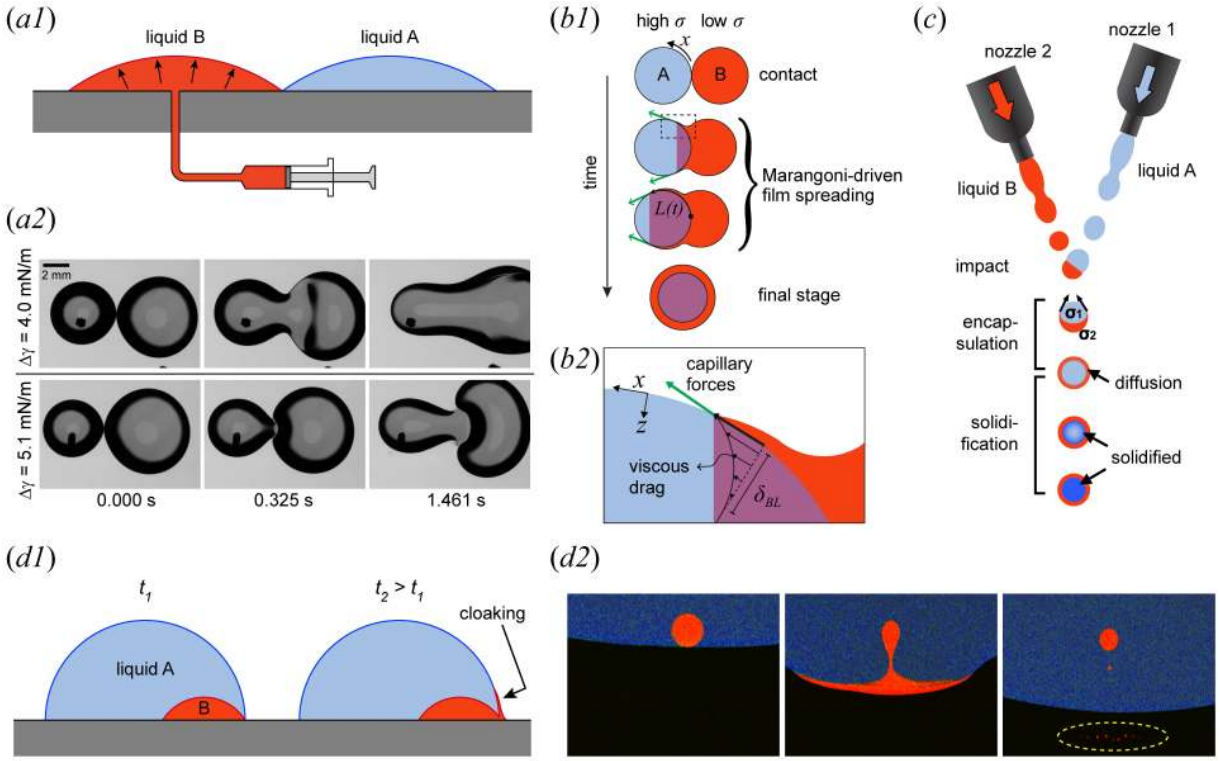

Figure 2: *Various types of coalescence of two droplets consisting of different liquids. In (a1) a side-view sketch of a coalescent experiment of two* sessile *droplets is shown [73, 74]. The outcome is shown in (a2), where we show top-view snapshots for two different surface tension differences* $\Delta\sigma$ *established with different 1,2-butanediol/water mixtures, featuring enhanced (upper row) respective delayed (bottom row) coalescence. Figures adapted from [73, 74]. In (b1) we sketch a side view of two* pendent *droplets [75], with the one with lower surface tension creeping over the one with higher surface tension. A detailed sketch of the process is shown in (b2), with the viscous velocity profile caused by the viscous force, counteracting the Marangoni force, which here however wins, leading to encapsulation. Sketches adapted from [75]. (c) Similarly, an encapsulation is also possible for* jetted *droplets of different liquids [76]. Here, one droplet contains a cross-linker and the other a polymer, such that the coalescence leads to solidification. In (d1) we sketch two snapshots (at two different times* t_1 *and* $t_2 > t_1$*) of another geometry of droplet-droplet interaction, namely one sessile droplet sitting on another smaller one. When the two three-phase-contact-lines touch each other (left,* t_1*), part of the smaller droplet can be "spit out" (right,* t_2*). Three actual snapshots of confocal images at consecutive times are shown in (d2). Figures adopted from [77].*

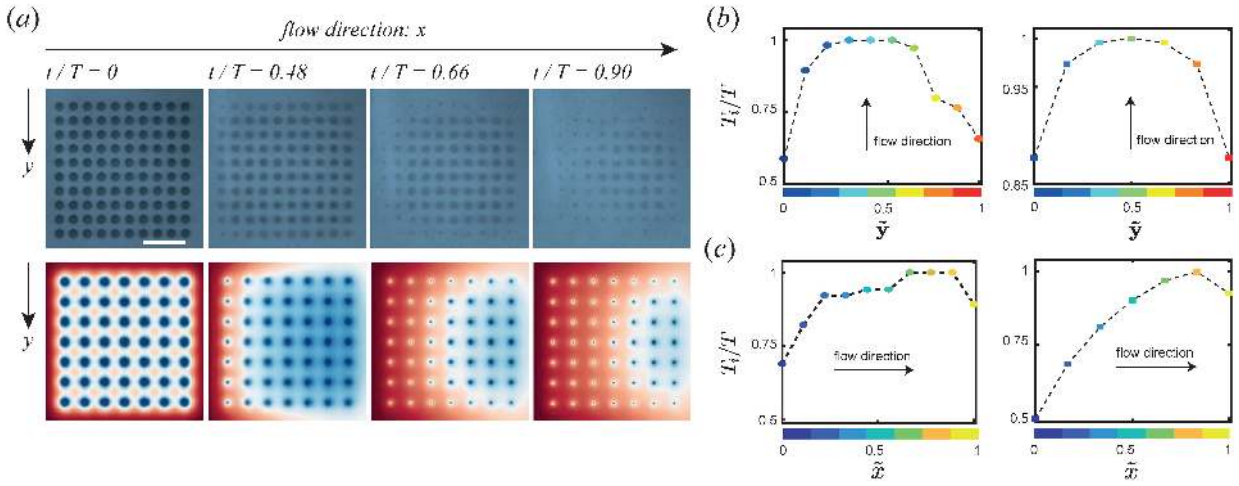

Figure 3: *Collective dissolution for droplets: (a) Time evolution of droplet dissolution: The upper row shows the experimental results for a 10×10 oil droplet array with a spacing of 5 μm for a flow rate of* $200\mu L/min$ *(corresponding to a Peclet number of* $Pe = 237$*) for four difference times* t*, normalized using* T*, which is the total time for the droplet array to completely dissolve. The length of the scale bar is 45 μm. The lower row shows a pseudocolour plot of the concentration field from numerical simulations for a 7×7 droplet array for corresponding flow conditions. Blue and red corresponds to oil and water, respectively. The water is injected into the chamber along the* $\hat{e}_x$ *direction. (b) Total dissolution time (*T_i*) of droplets along the span-wise direction y and (c) the stream-wise direction x. In (b) and (c), on the left the experimental data are shown, and on the right the numerical ones. Figures adapted from [42].*

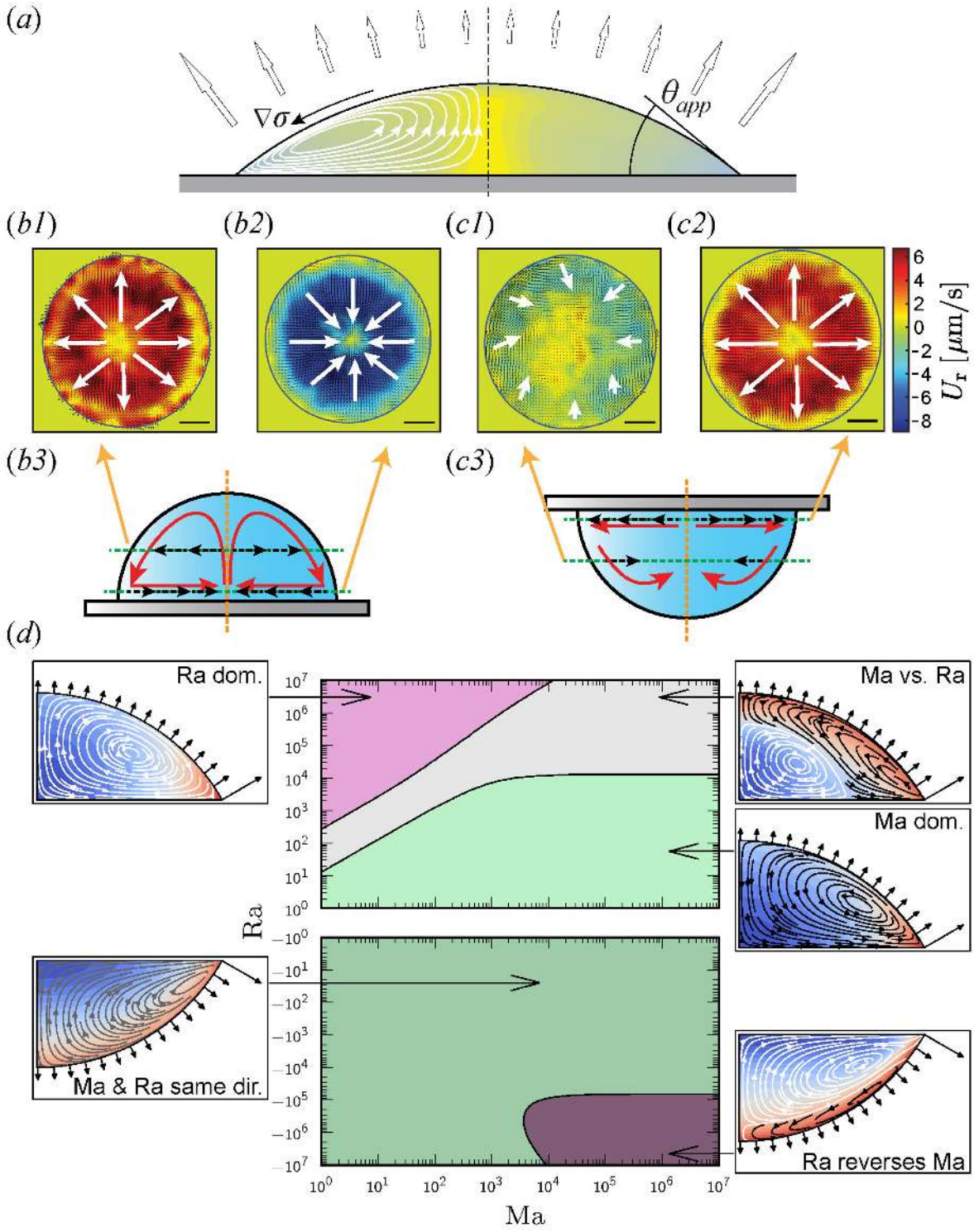

Figure 4: *(a) Evaporation of a 5 pL binary droplet consisting of ethanol (0.1%) and water. The higher evaporation rate at the rim and the selective evaporation of the ethanol leads to a surface tension gradient $\nabla\sigma$ at the droplet-air interface, driving Marangoni convection inside the droplet. Note that for larger driving (i.e., larger Marangoni number), the axisymmetry of the process breaks. The evaporation of a binary sessile (b) and of a binary pendant (c) droplet: (b1/c1) and (b2/c2) show the measured velocity field within the sessile/pendant droplet droplet at midheight/at the substrate, as shown in the side view sketches (b3/c3). The different flow patterns in (b) and (c) clearly reveal that gravity (pointing downwards) plays a major role. Figure taken from [40]. (d) Phase diagram in the Ra vs Ma parameter space for an evaporating binary droplet: Depending on Ra and Ma, either Rayleigh convection rolls are seen, or Marangoni convections rolls, or both. We also show the respective flow and concentration patterns. Figure taken from [136].*

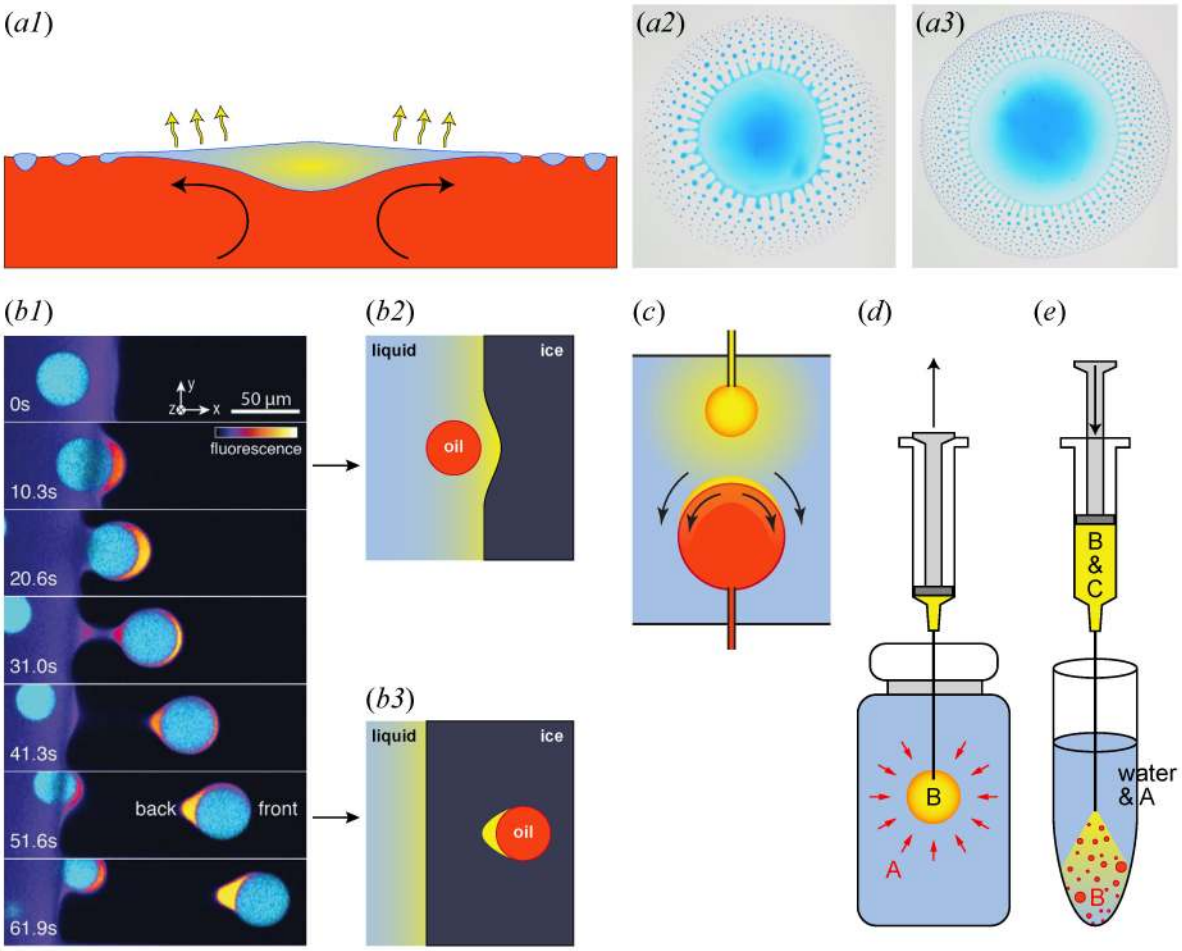

Figure 5: *(a) Marangoni bursting: Evaporation-induced emulsification of a two-component droplet (isopropanol and water) on an immiscible bath. (a1) Sketch of the mechanism. (a2) and (a3) Top view of the flow pattern for two different isopropanol concentrations of the deposited binary alcohol-water droplet, from lower ((a2), 0.4 mass fraction) to higher ((a3), 0.45 mass fraction). Figures taken from [139] (after adoption). (b1) Typical interaction between a droplet and the solidification front, showing the accumulation of solute and its redistribution around the droplet. Horizontal cross section. Here the temperature gradient leading to the freezing is 5 K/mm, with a sample velocity of 2µm/s. Figure taken from [141]. The sketches (b2) (early times) and (b3) (later times when the front has passed over the oil droplet) visualize the process. (c) Two droplets of two different slightly soluble liquid are approached to each other in a third liquid and interact diffusively, even before they coalesce. (d) Classical single droplet microextraction, as developed by Pregl [142]. (e) Principle of Dispersed Liquid-Liquid Microextraction (DLLME), as first suggested in ref. [143]. For an explanation we refer to the text.*

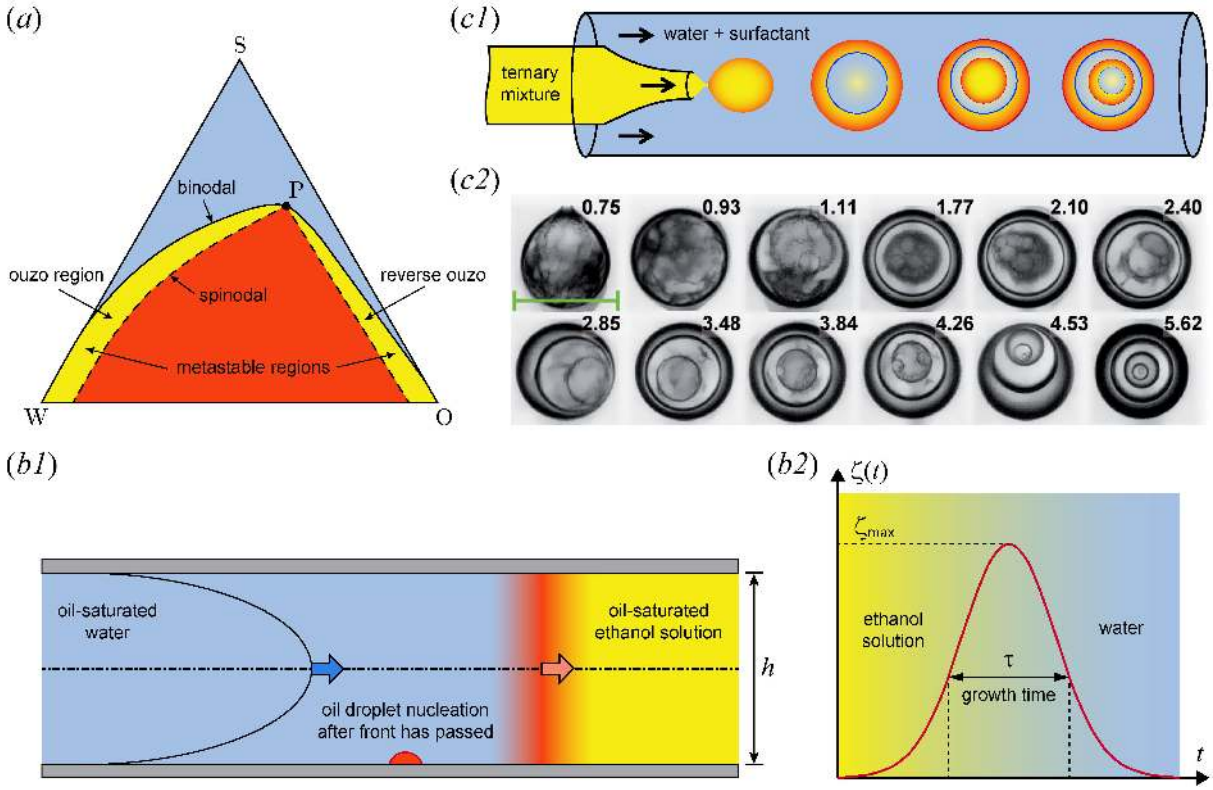

Figure 6: *(a) Schematic ternary diagram of a ternary mixture of water (w), a solute (S) like ethanol, and an oil (O) like anise oil in the case of ouzo. At the corners, the respective liquid has a 100% concentration. The concentration then linearly decreases to zero at the other two corners, along the axes of the triangle. Above the binodal curve, the three liquids are fully miscible (blue region). Below the spinodal curve (red region), water and oil separate into two phases. In between the binodal curve and the spinodal curve, there is a small region (yellow) in which sub-micrometer-sized oil droplets in water ("ouzo region") or water droplets in oil ("reverse ouzo") are metastable. Figure adapted from [158]. More complicated ternary diagrams with so-called pre-ouzo regimes with oil nanodroplets in an otherwise miscible regime are possible [159]. Principle of solvent exchange: (b1) A bad solvent (here water) is replacing a good solvent (here ethanol), leading to a front of oversaturation and thus to the nucleation of (here oil) droplets at the (hydrophobic) surface. Note that the plug-flow like nature of the oversaturation front is due to Taylor-Aris dispersion [160–163]. The velocity profile itself remains parabolic. (b2) For fixed position at the wall, a front of oversaturation $\zeta(t) > 0$ is passing by, leading to droplet growth. Figure adapted from [164]. (c1) Ternary liquid of oil, water, and ethanol brought into contact with an aqueous phase with a co-flow device [165, 166], leading to phase-separation in the emerging droplets, which develop onion-like structures. (c2) Details of the developing onion-like structures of a phase-separating ternary liquid of (a). The time is given in seconds. The length-scale given in the first snapshot at* $0.75s$ *is* $100\mu m$*. Figure taken from [167].*

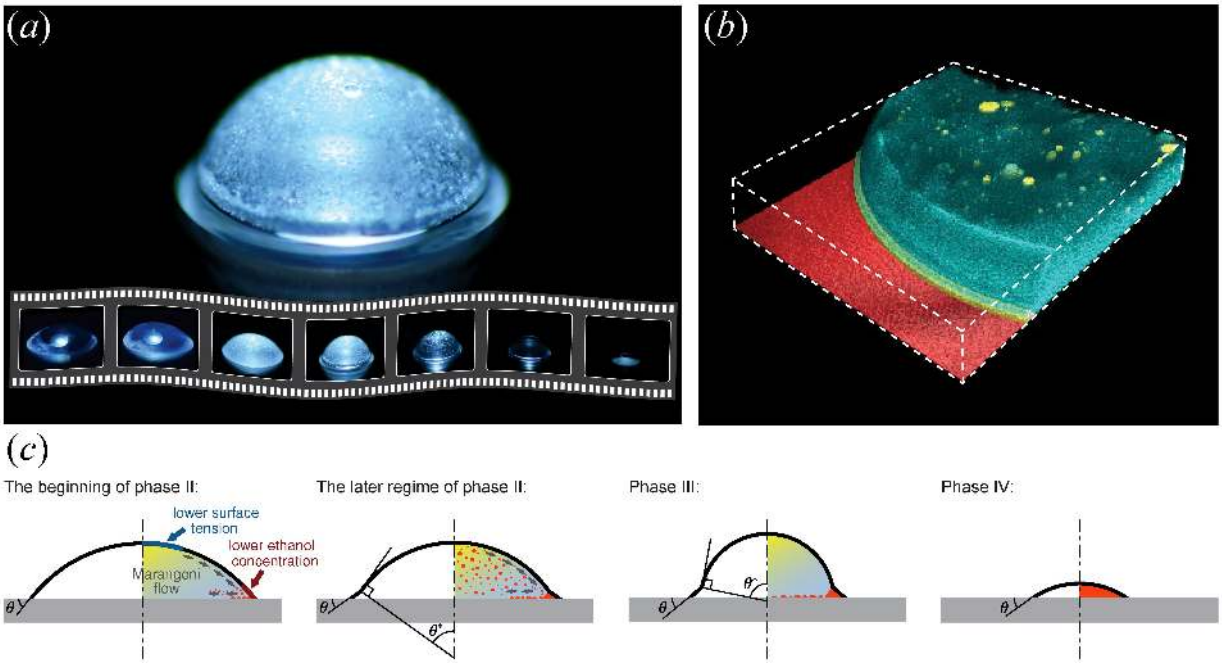

Figure 7: *Evaporating ouzo droplet: (a) Optical image of phase III of the droplet, with a milky droplet sitting on an oil ring. The seven insets show earlier and later snapshots of the droplet. (b) Confocal image early in phase III, when the oil ring starts to develop. (c) The four sketches show different lifetime phases of the evaporating ouzo droplet, see the text for more details. Figures adapted from [17].*